Wave run-up loads on the Main Access Platform of a monopile

Master Thesis

P.E. Wentink

Delft University of Technology

Wave run-up loads on the Main Access Platform of a monopile

by

P.E. Wentink

to obtain the degree of Master of Science
at the Delft University of Technology,
to be defended publicly on Tuesday May 6, 2025 at 09:00 AM.

Student number:	4543173	
Thesis committee:	Dr. ir. P. R. Wellens,	TU Delft, Chair
	Prof. G. D. Weymouth,	TU Delft
	Dr. ir. J. F. J. Pruijn,	TU Delft
	Ir. E. N. Klaver,	Van Oord
	Ir. H. W. Smaling,	Van Oord
	Ir. S. Bindiganavile Ramadas,	Van Oord

An electronic version of this thesis is available at `http://repository.tudelft.nl/`.

TUDelft

Summary

This document explores the wave run-up loads on offshore monopile structures, particularly those experienced by the main access platforms during severe storms. Such incidents have been observed to cause significant damage, necessitating a deeper understanding and accurate prediction of these loads. The main objective of this research is to compare various vertical wave run-up load models, focusing on their prediction accuracy and computational efficiency. First the wave run-up heights and wave run-up loads of analytical models are compared to each other. These results are calculated with the maximum wave heights and water depths on the Dogger Bank. It can be seen that the wave run-up heights and therefore the wave run-up loads are unrealistically high. The main reason for this is that the analytical models are used outside the boundaries where they are validated for. This leads to less reliable results. Theoretical and numerical limitations are in this thesis to increase the reliability of the results.

Contents

List of Figures

List of Tables

1

Introduction and Literature

Over the last decade more and more offshore wind turbines have been installed. In this period some of them have experienced high wave run-up on the monopile [5]. During severe storms the wave run-up becomes so high that the wave run-up hits the main access platform of the monopile. These hits could cause major damage to the platform. Since these hits occur [5], it is necessary to better understand under what circumstances they occur and how they can be predicted. In order to determine the vertical wave run-up loads on the main access platforms of monopiles, the first step is to determine the wave run-up height on the monopile. The next step is to translate these wave run-up heights into wave run-up pressures. In this chapter an overview of the available literature on analytical models and numerical models for the wave run-up and the resulting loads is given.

1.1. Introduction of key definitions

Three key definitions will be explained.

1. The main access platform of a monopile: refers to the platform on the monopile structure above the sea. This platform provides access to the inside of the monopile and the turbine to perform maintenance for example.
2. The wave run-up height on the monopile: when a wave passes through a wind farm it hits the monopile structures. This interaction between the wave and the structure causes the water to run-up and go around the monopile since it cannot go through. The wave run-up height is defined as the z-location of the wave run-up with respect to the mean sea water level.
3. The wave run-up loads: when a wave has a lot of energy, the wave run-up height can become as high as the main access platform of the monopile and hit the structure.

1.2. Literature review

The literature review is split up in three different parts. The analytical wave run-up height, the analytical wave run-up loads and the numerical part.

1.2.1. Wave theories

In this section Stokes' wave theory and Dean's stream-function theory are described, both theories describe non-linear waves. Since the waves in this research are extreme and therefore close to the breaking limit, linear wave theory is not adequate enough, see Figure 1.1.

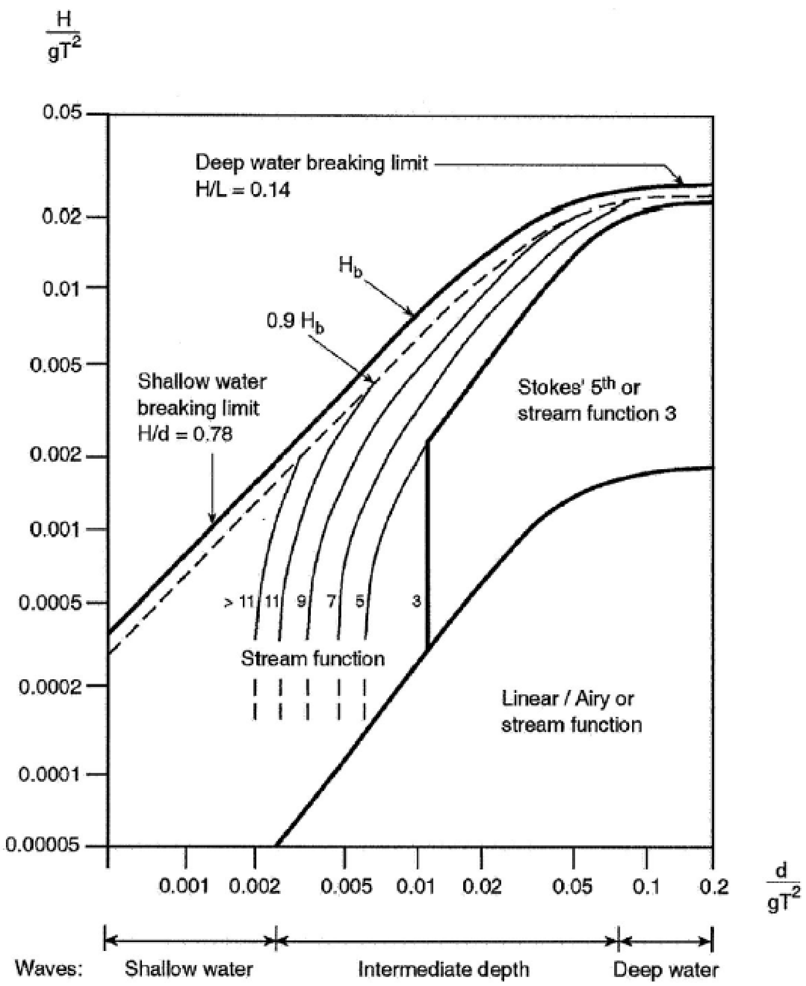

Figure 1.1: Graph from DNV whether when to use which wave theory. [8]

Stokes wave theory

Stokes Wave Theory, introduced by Fenton, 1988 [11], is an approach to describe nonlinear periodic waves on the surface of an inviscid, incompressible, and irrotational fluid. The theory proceeds by expanding the wave profile and fluid velocity potential as power series. In the theory of Stokes, the basic equation is written as:

$$\eta(x,t) = a\cos(\omega t - kx) = \varepsilon\eta_1(x,t) \tag{1.1}$$

where, the wave steepness is $\varepsilon = ak$ and $\eta_1(x,t) = k^{-1}\cos(\omega t - kx)$. The first correction in the Stokes theory is an extra harmonic wave, written with the wave steepness raised to the second power.

$$\eta(x,t) = \varepsilon\eta_1(x,t) + \varepsilon^2\eta_2(x,t) \tag{1.2}$$

where $\varepsilon\eta_2$ represents the extra harmonic wave. The solution of this equation is:

$$\eta(x,t) = a\cos(\omega t - kx) + ka^2\frac{\cosh(kd)}{4\sinh^3(kd)}[2 + \cosh(2kd)]\cos[2(\omega t - kx)] \tag{1.3}$$

where the first term is the linear part and the second term is the second-order Stokes correction. A visual representation is given in Figure 1.2.

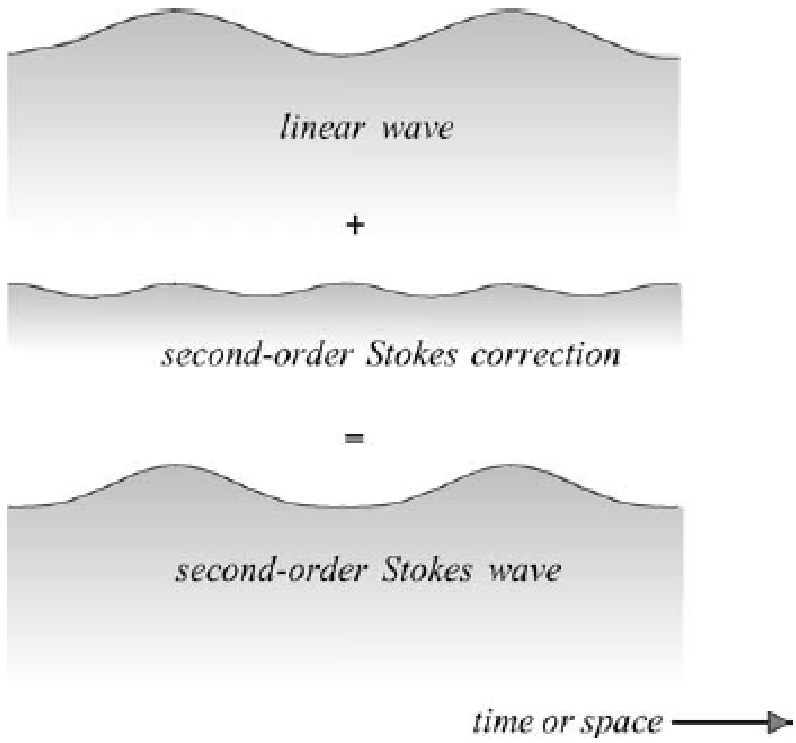

Figure 1.2: Visual representation of Stokes wave theory [15]

This approximation can be expanded indefinitely to higher orders to get a better representation.

$$\eta = \varepsilon\eta_1 + \varepsilon^2\eta_2 + \varepsilon^3\eta_3 + \varepsilon^4\eta_4 + \varepsilon^5\eta_5 + \cdots \tag{1.4}$$

The equations are from the book Waves in Oceanic and Coastal Waters by Holthuijsen., 2007 [15].

Stream-function wave theory
In the stream function theory the velocity components and the surface profile are written in terms of a series of harmonics (depending on the desired order of approximation). The nonlinear basic equations are not solved with the velocity potential but with another function: the stream function ψ. This stream function is described as:

$$\begin{aligned} \frac{\partial\psi}{\partial z} &= u_x \quad \left(= \frac{\partial\phi}{\partial x}\right) \\ -\frac{\partial\psi}{\partial x} &= u_z \quad \left(= \frac{\partial\phi}{\partial z}\right) \end{aligned} \tag{1.5}$$

If the stream function is visualised as a hill above a horizontal x, z-plane, then the particle velocities are oriented along the contour lines of the hill, and their magnitudes are equal to the slope of the hill in the direction normal to these contour lines. The existence of a stream function implies that the continuity of the water mass in two dimensions is always guaranteed, because

$$\frac{\partial u_x}{\partial x} + \frac{\partial u_z}{\partial z} = \frac{\partial^2\psi}{\partial z\partial x} - \frac{\partial^2\psi}{\partial x\partial z} = 0 \tag{1.6}$$

The equations are from the book Waves in Oceanic and Coastal Waters by Holthuijsen., 2007 [15].

1.2.2. Analytical wave run-up height on cylinders

A considerable amount of studies have investigated the wave run-up on vertical cylinders. In this section the developments in the analytical approach are explained.

Hallermeier, 1976 [14] proposed a formula for the prediction of wave run-up on vertical cylinders based on the velocity stagnation head theory. The idea of this theory is that when the wave hits the structure, the kinetic energy of the water particles at the wave crest has to be converted into potential energy by rising the distance $u^2/2g$ above the crest level. The crest level refers to the highest point of a wave above the still water level, the water level serves as a reference point for measuring wave heights. The following formula is proposed:

$$R_u = \eta_{max} + \frac{u^2}{2g} \tag{1.7}$$

where R_u is the run-up height on the vertical cylinder $[m]$, η_{max} the maximum wave crest elevation $[m]$, u^2 the horizontal water particle velocity $[m/s]$ and g the gravitational acceleration $[m/s^2]$.

De Vos et al., 2007 [7] conducted small scale experiments on vertical cylinders. Using the second order Stokes theory for the wave kinematics, the velocity stagnation head theory is adjusted with the run-up coefficient m as proposed by Niedzwecki and Duggal, 1992 [21] to obtain the prediction formula for the run-up caused by regular waves. The formula becomes:

$$R_u = \eta_{max} + m \cdot \frac{u^2}{2g} \tag{1.8}$$

where R_u is the run-up height on the vertical cylinder $[m]$, η_{max} the maximum wave crest elevation $[m]$, m run-up coefficient [-], u^2 the water particle velocity $[m/s]$ and g the gravitational acceleration $[m/s^2]$. De Vos et al., 2007 [7] found that a value of $m = 2.71$ [-] gives a good estimation of the wave run-up height in irregular waves.

The data from De Vos et al., 2007 [7] has been reanalyzed by Lykke Andersen et al., 2011 [20]. The study uses the stream function theory introduced by Fenton, 1988 [11]. This research is also validated for irregular waves. In their research they came up with the following design rules for wave run-up:

$$R_{u,\max} = \eta_{\max} + 1.4 \cdot m \cdot \frac{u_{\max}^2}{2g} \tag{1.9}$$

where $m = 4$ for $s_{0p} = 0.02$ and $m = 3$ for $s_{0p} = 0.035$. This gives less scatter and on average an increase of the value m.

Ramirez et al., 2013 [26] improved the formulations from Lykke Andersen et al., 2011 [20]. They studied wave run-up on vertical piles by conducting large scale experiments. Only the irregular wave from these experiments are considered for the research. The wave run-up is divided in three different levels, all with their own formulation of m. The run-up levels are divided in the following way, these levels are shown in figure 1.3:

- Level A: Level for green water run-up (thick layer)
- Level B: Level for thin layer of water and air mixture, water layer which is no longer attached to the surface of the pile or high spray concentration.
- Level C: Level for maximum spray. When the spray went higher than the maximum level which was marked on the pile, this value was estimated as good as possible.

The results of m are given per level and with a condition for the peak wave steepness:

$$s_{0p} = \frac{2\pi H_{m0}}{gT_p^2} \tag{1.10}$$

where H_{m0} is the significant wave height in the frequency domain $[m]$, g is the gravitational acceleration $[m/s^2]$ and T_p is the peak wave period $[s]$. The expressions are the following:

- Level A:

$$m = \begin{cases} -66.667 s_{0p} + 5.33 & \text{for } s_{0p} < 0.035 \\ 3 & \text{for } s_{0p} > 0.035 \end{cases} \tag{1.11}$$

- Level B:

$$m = \begin{cases} -93.333 s_{0p} + 7.47 & \text{for } s_{0p} < 0.035 \\ 4.2 & \text{for } s_{0p} > 0.035 \end{cases} \tag{1.12}$$

- Level C:

$$m = \begin{cases} -200 s_{0p} + 16 & \text{for } s_{0p} < 0.035 \\ 9 & \text{for } s_{0p} > 0.035 \end{cases} . \tag{1.13}$$

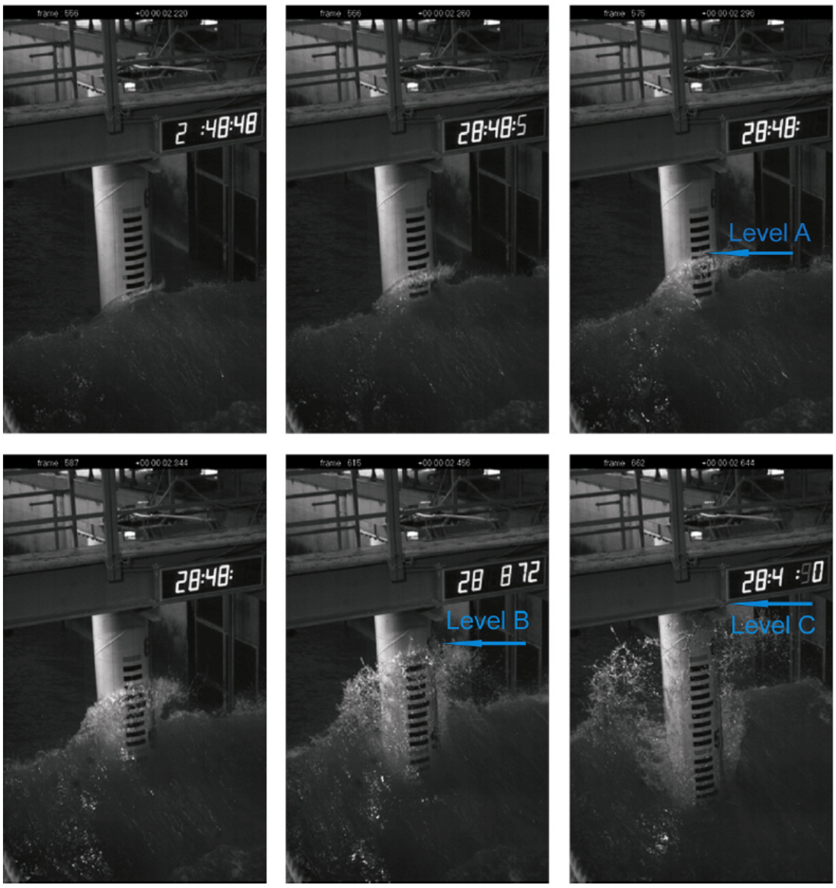

Figure 1.3: Different run-up levels in the study of Ramirez et al., 2013 [26]

Kazeminezhad and Etemad-Shahidi, 2015 [17] investigated the data set from experiments carried out by Lykke Andersen, 2007 [19], De Vos et al., 2007 [7] and Ramirez et al., 2013 [26]. In their studies they did not make use of the velocity stagnation head theory, but instead they estimated the wave run-up height based on non-dimensional wave parameters for regular waves:

$$\frac{R_u}{H} = 0.76 \left(\frac{H}{h}\right)^{0.15} \left(\frac{H}{L_0}\right)^{-0.055} \quad for: \frac{H}{h} \leq 0.41 \tag{1.14}$$

$$\frac{R_u}{H} = 0.65 \left(\frac{H}{L_0}\right)^{-0.055} + 3.2 \times 10^{-3} \left(\frac{H}{h} - 0.41\right)^{0.15} \left(\frac{H}{L_0}\right)^{-1.5} \quad for: \frac{H}{h} > 0.41 \tag{1.15}$$

where H is the wave height $[m]$, h the water depth $[m]$ and L_0 the deep water wave length $[m]$.

Bonakdar et al., 2016 [3] continued with this research and included a shallow water condition since these were missing in the research done by Kazeminezhad and Etemad-Shahidi, 2015 [17]. Also the relative diameter is included in the equations, D/L. This is an extra relation that is included and fitted to the experiments for more accurate wave run-up results. Bonakdar et al., 2016 [3] only focused on regular waves and thus disregarded previous findings on irregular waves.

$$\frac{R_u}{H} = 0.863 \left(\frac{H}{h}\right)^{0.117} \left(\frac{h}{L}\right)^{-0.206} \left(\frac{D}{L}\right)^{0.108} \quad for: \frac{H}{h} \leq 0.41 \tag{1.16}$$

$$\frac{R_u}{H} = 0.777 \left(\frac{h}{L}\right)^{-0.206} \left(\frac{D}{L}\right)^{0.108} + 0.138 \left(\frac{H}{h} - 0.41\right)^{0.316} \left(\frac{h}{L}\right)^{-2.6} \left(\frac{D}{L}\right)^{1.16} \quad for: \frac{H}{h} > 0.41 \tag{1.17}$$

where H is the wave height $[m]$, h the water depth $[m]$, D the cylinder diameter $[m]$ and L the wave length $[m]$.

In 2017, de Latour [6] continued research with the raw data collected during the Join Industry Project WIFI JIP II. This is data on wave run-up height on a cylinder. During this research de Latour continued with the approach of Bonakdar et al., 2016 [3]. They propose equations for use in irregular waves instead of regular waves. The formulas are tested with the experiments performed during the Joint Industry Project and show good results because they are fitted to the experiments.

$$\frac{R_{u,\max}}{H_{\max}} = 2.5\left(\frac{H_{\max}}{h}\right)^{0.117}\left(\frac{h}{L_{\max}}\right)^{-0.206}\left(\frac{D}{L_{\max}}\right)^{0.108} \text{for: } \frac{H}{h} \leq 0.36 \tag{1.18}$$

$$\begin{aligned}\frac{R_{u,\max}}{H_{\max}} = 1.4\left(\frac{h}{L_{\max}}\right)^{-0.206}&\left(\frac{D}{L_{\max}}\right)^{0.108}\\ &+ 0.93\left(\frac{H_{\max}}{h} - 0.36\right)^{0.316}\left(\frac{h}{L_{\max}}\right)^{-2.6}\left(\frac{D}{L_{\max}}\right)^{1.16} \quad \text{for: } \frac{H}{h} > 0.36\end{aligned} \tag{1.19}$$

where H_{max} is the maximum wave height $[m]$, h the water depth $[m]$, D the cylinder diameter $[m]$ and L_{max} the maximum wave length $[m]$.

Garborg et al., 2020 [12] performed a large re-analysis of the irregular waves of the small scale model tests of Lykke Andersen et al., 2011 [20] and large-scale model tests of Ramirez et al., 2013 [26]. They found that the wave run-up is strongly dependent on the wave non linearity. The run-up coefficients are chosen to be constant for level A, B and C for the sake of simplicity. They are found using stream function wave theory. For Level A: $m = 1.5$, Level B: $m = 3.0$ and for Level C: $m = 5.0$.

Grue and Osyka, 2021 [13] found in their investigation that the highest run-up was achieved when the wave breaks violently just behind the monopile. Next to that the measured run-up velocity shows a strong nonlinear relationship with the wave slope. Breaking waves are however not considered in this research.

Li et al., 2022 [18] investigated the wave run-up influential factors. They carried out regular wave experiments. They defined a new form for m:

$$m = 0.812(A/D)^{-0.584}(0.239ka + 0.947) \tag{1.20}$$

They found that the wave steepness and the structural parameters, ka and A/D, where k is the wave number, a is the radius of cylinder [m], A is the wave amplitude [m] and D is the diameter of the cylinder [m], significantly affect the wave run-up. Particularly, for the parameter A/D, the previous formulae proposed in literature did not include its effect on the wave run-up. They improved the wave run-up coefficient based on the velocity stagnation head theory.

1.2.3. Analytical wave run-up loads

Literature of the wave run-up loads on the main access platforms on monopiles exists, but in contrast to the wave run-up there is far less research available. This section describes various analytical formulas used to determine the wave run loads on a platform.

In 2007 Lykke Andersen and Brorsen, 2007 [19] have measured pressures on horizontal and conical platforms in a small scale model for irregular waves. By comparing these results with run-up tests performed earlier, slamming coefficients have been calculated. They observed that irregular and possibly breaking waves cause more slamming. The first step to calculate the pressures on the horizontal platform is to calculate the run-up velocity:

$$v(z) = \sqrt{2g \cdot (R_u - z)} \tag{1.21}$$

where $v(z)$ is the run-up velocity at the vertical coordinate z [m/s], g the gravitational acceleration $[m/s^2]$, R_u the run-up height [m] and z is the vertical coordinate with respect to the reference level [m]. They use the results of this equation and the measured pressures on the platform to derive the slamming coefficients. An example of these slamming coefficients can be found in figure 1.4. They are found to be significantly larger than coefficients of regular and mainly non-breaking waves.

In Damsgaard et al., 2007 [5] the pressure on the horizontal platform is calculated, in this calculation the slamming coefficient C_s is included:

$$\frac{F}{A} = \frac{1}{2} C_s \rho (v(z))^2 \tag{1.22}$$

where ρ is the seawater density $[kg/m^3]$ and $v(z)$ is the run-up velocity at the vertical coordinate z [m/s]. During their research they also found that the loads on the horizontal platform are twice as high as the loads on a conical platform with a slope of 45 degrees.

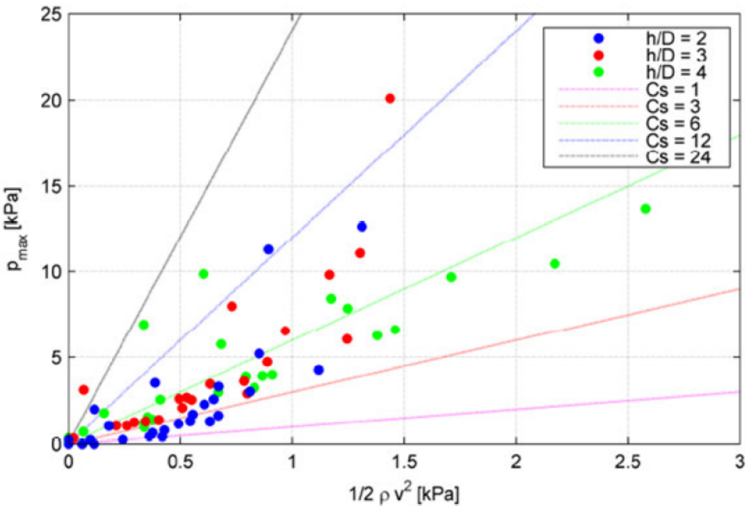

Figure 1.4: Measured pressures for the horizontal platform indicating the slamming coefficient for the maximum local load, from Damsgaard et al., 2007 [5]

Another method to estimate the vertical wave load is developed by Abdussamie et al., 2014 [2].

$$F_z(t) = \frac{\pi}{8} \rho \frac{Bl^2}{\left[1 + \left(\frac{l}{B}\right)^2\right]^{1/2}} \dot{w} + \frac{\pi}{4} \rho Bl \frac{dl}{dt} \frac{1 + 0.5\left(\frac{l}{B}\right)^2}{\left[1 + \left(\frac{l}{B}\right)^2\right]^{3/2}} w \quad + 0.5 \rho Bl C_D w|w| + \rho Bl(\eta - a)(g + \dot{w}) \tag{1.23}$$

where the first, second and third terms represent the inertial force, the impact/slamming force and the drag force respectively. The wave kinematics, particle velocity and acceleration in z-direction, are denoted by w and $\dot{w}$. The parameter l denotes the horizontal wetted length of the platform, η represents the instantaneous wave elevation, B the breadth of the deck structure, C_D is the drag coefficient and ρ is the seawater density.

The results from this equation have been compared with experiments and a CFD model. This new equation is slightly underestimating the vertical loading but is accurate enough to use for a quick estimation. But is not further used because it is only a platform above the water line, no wave run-up on a cylinder is there prior to impact.

1.2.4. Numerical wave run-up

In this section the numerical approach of calculating the wave run-up on the monopile is discussed.

Bredmose and Jacobsen, 2011 [4] performed a 3-dimensional numerical investigation of wave interaction with a monopile and a main access platform. In their study it has been found that the lowest platform elevation resulted in the highest forces on the platform. The results of their investigation can be found in figure 1.5. They also mentioned that the point of wave overturning was influenced by the grid resolution.

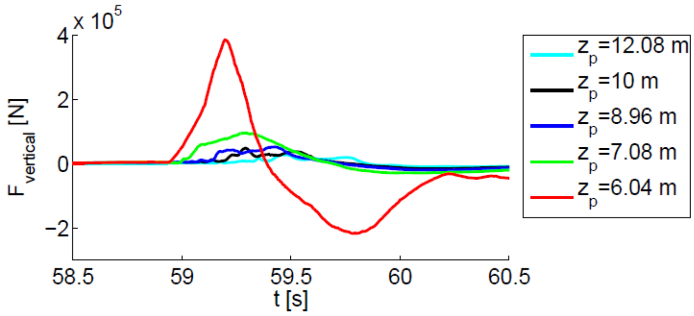

Figure 1.5: Vertical forces on main access platform from Bredmose and Jacobsen, 2011 [4]

Noticing the more accurate result using non-linear theory found in the study of Lykke Andersen et al., 2010 [20], Peng et al., 2012 [25] decided to compare a CFD model with these results. They found that the wave run-up is strongly dependent on the wave non-linearity. Next to this they found that the relative wave run-up is strongly dependent on the Ursell number, the following relation is found:

$$\frac{R_u}{h} = 10.8 \cdot \gamma_D \cdot \ln\left(0.27 \cdot \mathrm{U_r} + 1\right) \tag{1.24}$$

where γ_D is a factor accounting for the effect of structure diameter on wave run-up and U_r, Ursell number calculated as $U_r = \frac{HL^2}{h^3}$, U_r depends on the wave height H [m], wave length L [m] and water depth h [m].

Pavilons et al., 2022 [24] performed a study of which the objective was to find the waves within a sea state that lead to the largest hydrodynamic loads on a 2D representation of a main access platform. The numerical wave tank used can be found in figure 1.6. They found that the wave with the highest surface elevation and the largest breaking index leads to the largest hydrodynamic loads if it overturns within a distance of approximately $1/3\lambda_p$ before the location of the platform. This leads to the following wave selection range for breaking waves in OceanWave3D [10]

$$-\frac{2}{3}\lambda_p + x_{B85} < x_{\mathrm{T}} < \lambda_p + x_{B85} \tag{1.25}$$

with λ_p representing the wave length associated with the peak frequency of the spectrum, x_{B85} the location of breaking onset and x_{T} the location of the structure. They also mentioned that the surface elevation is the best screening parameter for the maximum moment at the wave's incipient point.

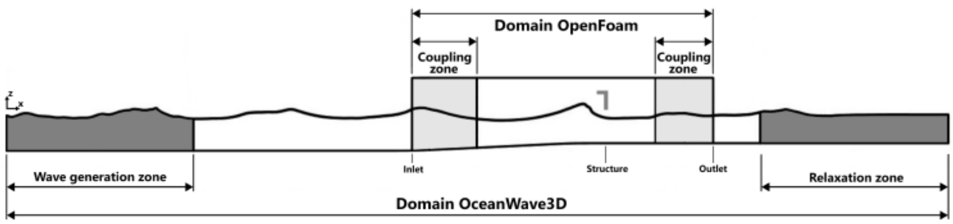

Figure 1.6: Sketch of the 2D numerical wave tank used in Pavilons et al., 2022 [24]

In OpenFOAM it is possible to measure forces on a surface, this is typically done using the forces or forceCoeffs function object. During the simulation, OpenFOAM calculates the pressure and shear stress distributions on these surfaces. The integral of the pressure over a surface, combined with the surface normal directions, contributes to the net pressure force. The function object outputs force data at specified time intervals, so it is possible to track the forces over time.

1.3. Problem description

As discussed above, literature is available for the wave run-up heights on a monopile for both analytical and numerical methods. However, there is little literature on the loads on main access platforms that follow from these wave run-ups. Within the industry, the challenge lies in the multitude of methodologies available for calculating wave run-up velocity and with that the loads, with analytical approaches. Furthermore, the outcome differs significantly with 3D numerical methods.

Numerical models, especially in 3D, are known to be very time consuming and need a huge amount of computational power. Therefore, early on in the design, the platform needs to be fixed in shape and elevation. Hence, it is desirable to have a reliable relatively quick method to estimate the wave run-up loads that could be used in earlier phases of design works.

2 Research objectives and Methodology

The objective of this research is to compare different vertical wave run-up load models. A comparison will be made on the differences in vertical load prediction and computational time. The results of this comparison will be used to obtain a model that can be used in the early design phase of monopiles where flexibility in main access platform shape and elevation is needed.

2.1. Research question

How can CFD modelling in OpenFOAM be applied to determine the wave run-up loads on the main access platform of a monopile in early design stage and how does this CFD model compare to existing analytical models?

2.1.1. Sub-questions

The following sub-questions support the main research question and will be answered throughout this research:

- How do the analytical wave run-up height models of Garborg et al., 2020 [12], de Latour, 2017 [6] and Li et al., 2022 [18] compare to each other?
- How are the wave run-up heights translated into loads?
- How does a numerical model in OpenFoam [16] compare to these analytical models?
- Is it possible to make a simple model to obtain reasonable accurate predictions (within a factor 2 on the conservative side) of wave run up loads within a time span of a few days?

2.2. Methodology and plan of approach

The following steps will be taken to reach the objective of this research:

1. Select a wind farm location that will be used in this study and describe the metocean parameters.
2. How do the analytical wave run-up height models of Garborg et al., 2020 [12], de Latour, 2017 [6] and Li et al., 2022 [18] compare to each other?
3. Calculate the wave run-up loads on the main access platform resulting from the wave run-up heights models from Garborg et al., 2020 [12], de Latour, 2017 [6] and Li et al., 2022 [18].
4. Use OceanWave3D by Engsig-Karup et al., 2009 [10] to create the individual waves needed for the numerical model.
5. Use the numerical model OpenFOAM to solve for the complex interaction between free surface flows and the structure.
6. Validate the results of the created numerical model against existing experimental data.
7. Compare the results of the created model with those from literature (both analytical and numerical) to obtain the optimum between, computational time and reliability.

The validation of this numerical model can be done using available experiments and models.

First of all, the wave run-up height can be validated with experiments done during the Wifi JIP II. In the experimental tests, run-up height on the monopiles were measured with wave gauges situated around the monopiles.

Secondly, in experiments from Andersen et al., 2007 [19] the pressure on the main access platform has been measured. Seventeen pressure sensors have been measuring the pressure at different places on the platform in this research. For each case the wave height, peak period, water depth, wave steepness, monopile diameter and platform height are mentioned as well.

3
Comparison analytical models

In this chapter the different analytical wave run-up height and load models are compared. First the wave run-up height of each model on a specific location will be compared, after that the wave run-up loads of each model on a specific location will be compared. The following analytical theories will be compared in this study: a method developed by de Latour, 2017 [6], developed after WIFI JIP II, the re-analysis Garborg et al., 2020 [12], the analysis done for the Dogger Bank wind farm, 2022 [9] and the theory Li et al., 2022 [18] developed.

3.1. Wind farm

In this section the location of the reference wind farm used in this study will be discussed. After that the metocean parameters used in this study will be explained.

3.1.1. Wind farm location

The reference site used in this study is the Dogger Bank wind farm. The seabed level within the wind farm range between -21 and -35 m LAT.

Figure 3.1: Location of the Dogger Bank.

3.1.2. Metocean parameters

The following metocean parameters data is available for each of the turbine in this location:

- $H_{m0,50}$: is the significant wave height over 50 years in the frequency domain. This is given as: $H_{m0} = 4\sqrt{m_0}$, where m_0, the zeroth moment of the variance spectrum, is obtained by integration of the variance spectrum.
- $H_{max,50}$: is the maximum wave height over 50 years in the time domain.
- T_p: is the peak wave period. The peak wave period corresponds with the wave period with the highest energy and corresponds with the peak of the wave spectrum.
- h: is the water depth. Defined as the vertical distance between the sea bottom and the still water level $[m]$
- D: is the diameter of the monopile $[m]$.
- SWL: is the still water level. It is used as a reference level.

With these available parameters, all other parameters needed for the calculations can be calculated using stream function theory. In Figure 3.2 the reference levels used in this study are drawn.

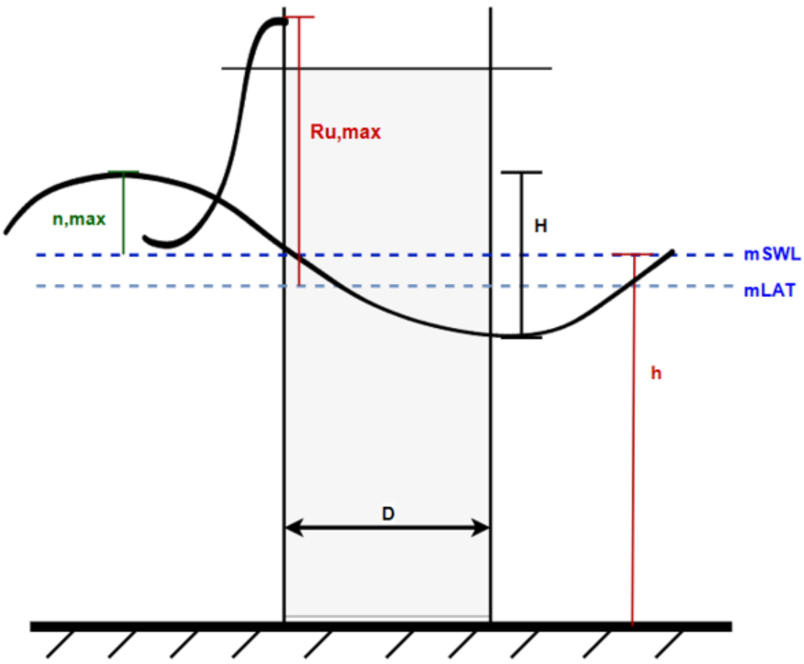

Figure 3.2: Reference levels

3.2. Wave run-up height

The formulas for the wave run-up height that will be compared can be found in table 3.1. For this research the value $m = 5$ for level C as proposed by Garborg et al., 2020 [12] is neglected. They mention that large variation is found in the maximum spray values, see figure 1.3. Another reason to not include level C wave run-up heights is that this research focuses on high impact loads, this spray consists of relatively small drops of water over a large area. This will not give high loads.

Table 3.1: Formulas in the comparison

Garborg	$R_u = \eta_{max} + m \cdot \frac{u^2}{2g}$ with: m = 1.5 for lvl A and m = 3.0 for lvl B
Garborg with m=3.5	$R_u = \eta_{max} + m \cdot \frac{u^2}{2g}$ with: m = 3.5
de Latour	$\frac{R_{u,\max}}{H_{\max}} = 2.5 \left(\frac{H_{\max}}{h}\right)^{0.117} \left(\frac{h}{L_{\max}}\right)^{-0.206} \left(\frac{D}{L_{\max}}\right)^{0.108}$ for: $\frac{H}{h} \leq 0.36$ $\frac{R_{u,\max}}{H_{\max}} = 1.4 \left(\frac{h}{L_{\max}}\right)^{-0.206} \left(\frac{D}{L_{\max}}\right)^{0.108} + 0.93 \left(\frac{H_{\max}}{h} - 0.36\right)^{0.316} \left(\frac{h}{L_{\max}}\right)^{-2.6} \left(\frac{D}{L_{\max}}\right)^{1.16}$ for: $\frac{H}{h} > 0.36$
Li	$R_u = \eta_{max} + m \cdot \frac{u^2}{2g}$ with: m=$0.812(A/D)^{-0.584}(0.239ka + 0.947)$

First, the steps that are taken in the model are explained to calculate the wave run-up height:

1. In this case the input for the model is coming from the Dogger Bank [1]. The input file consists of the 101 wind turbine location, the water depth (h) of the location and the corresponding maximum wave height over 50 years ($H_{max,50}$). Water depths for the Dogger Bank vary between -23.3 [m] and -34.44 [m]. The maximum wave heights vary between 16.1 [m] and 19.3 [m].
2. Since the wave period has not been provided for each wind turbine, a study has been performed [1] to see which period occur within the wind farm. It was found that the wave periods ($T_{H,max}$) are between 11.4 [s] and 18 [s]. Therefore in the model, for each wind turbine, the wave length (L) is calculated for the range of wave periods. In this research the wave periods are determined between 11.4 [s] and 18 [s] with steps of 0.1 [s]. The interval of these wave periods represents the wave periods associated with the 50 year maximum wave height in an extreme sea state. These associated wave periods are higher than the peak periods of the waves. These wave lengths are calculated with formula 3.1
$$L = \frac{gT^2}{2\pi} * \tanh(\frac{2\pi h}{L}) \tag{3.1}$$
This means an initial guess of L will be taken and an iterative process will take place to find the solution for which L converges. These values of wave length are stored for each wave period. In figure 3.3 the wave length, wave run-up height, surface elevation and maximum crest velocity are plotted versus the wave period for a steady maximum wave height value.

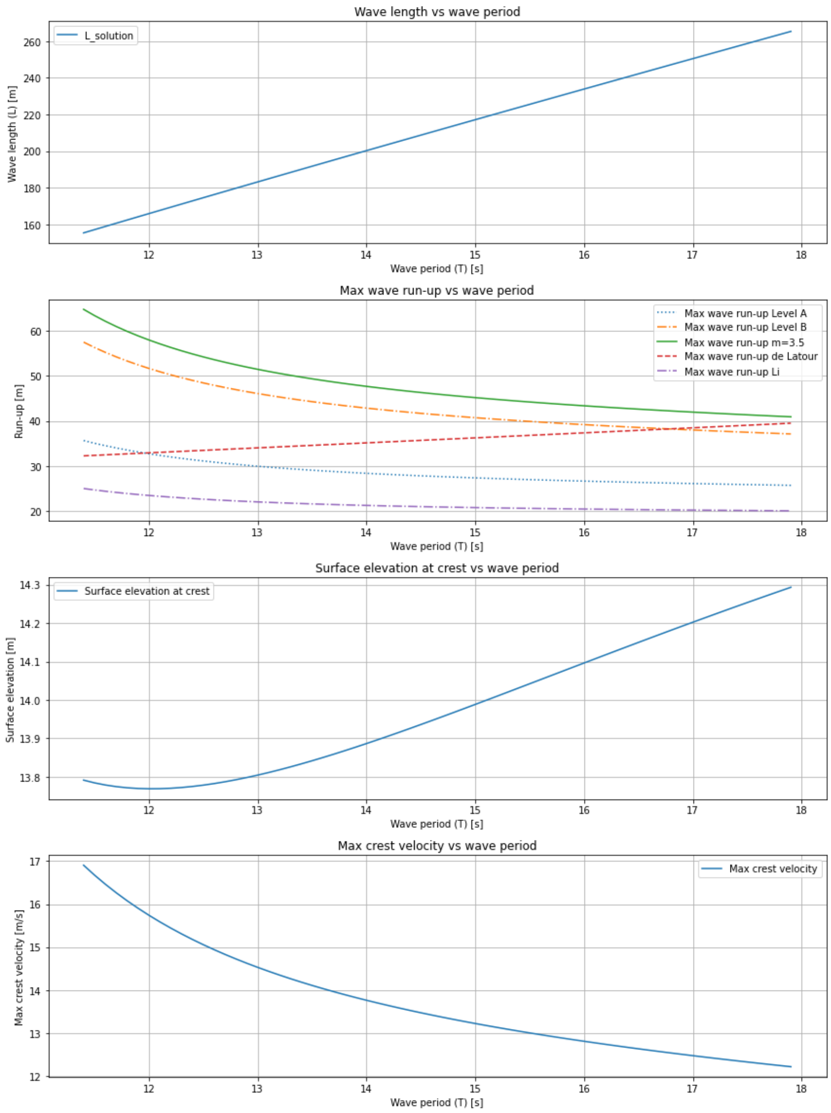

Figure 3.3: Wave length, maximum wave run-up height, surface elevation at the crest and maximum crest velocity vs T - H=18.29m, h=24.95m and D=8.5m

As shown in the figure there is a linear relation between the wave period and the wave length. A higher wave period will result in a higher wave length.

Another thing to point out is that for smaller wave periods and thus wave lengths the maximum crest velocity is higher. And therefore results in higher wave run-up heights.

3. In the next step the following wave characteristics needed for the formulas given in table 3.1 are calculated. The wave number (k), maximum crest velocity (u_{max}) and maximum surface elevation (η_{max}) are calculated using Fenton's stream wave function [11]. According to Holthuijsen [15] steam-function theory works well for non-linear waves. It captures higher-order non-linear waves for shallow and intermediate water depths. This means the wave characteristics will be calculated accurately for the waves within the wind farm. DNV provided the industry with guidelines on what stream function order to use for errors with a maximum of one percent, this can be seen in figure 3.4. The red dot in the figure is showing an example for the following case: $H = 15m$, $T = 15s$ and $h = 30m$. Since this case is representative for the wind turbine locations, it can be expected that a stream function order of 11 or higher is needed to accurately calculate the wave characteristics.

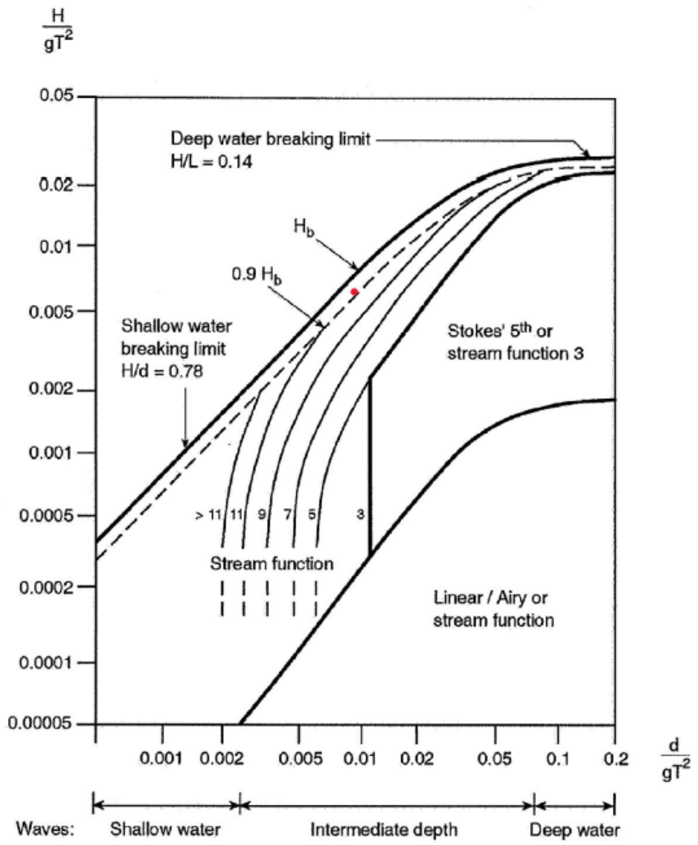

Figure 3.4: Applicable wave theories for different water depths [8]. The red dot represents the following wave: H=15m, h=30m and T=15s

4. As explained in step 3 the order N of the stream function is important for accurate estimations. The goal is to get a wave that satisfies the boundary conditions, requirements of convergence and consistency. To ensure this correct solution for the wave is reached, the surface elevations of the wave should not include any non-linearities, second peaks for example. The particle velocities over depth should hardly have any difference for different stream function orders. The last check is to check if wave length convergence is reached when increasing the stream function order.
5. When a correct stream function wave is found, the correct wave characteristics are calculated. All these parameters are inserted in the formulas mentioned in table 3.1. The model also creates an output file, this output file contains all information regarding each wind turbine. Each turbine returns for each method the wave period for the highest run-up height, the order used in the stream function and the highest wave run-up height.

For each method and turbine the highest wave run-up is plotted in the scatter plot in figure 3.5. As discussed before four of the five are based of the same formulas but are calibrated with the value m, and the formulas from de Latour, 2017 [6] is something different.

The first thing of notice is that the highest wave run-up heights are found in the shallower areas. This can be explained by the effect that in shallower areas, waves tend to get steeper. And steeper waves have been linked to higher wave run-up heights.

The second thing of notice is the lower values for the method developed by Li et al. The figure shows that almost all values are lower than the values of Garborg level A. This means that all wave run-up heights from Li are lower than the thick layer wave run-up (see figure 1.3). In the next section a sensitivity analysis is performed to find the reason for this.

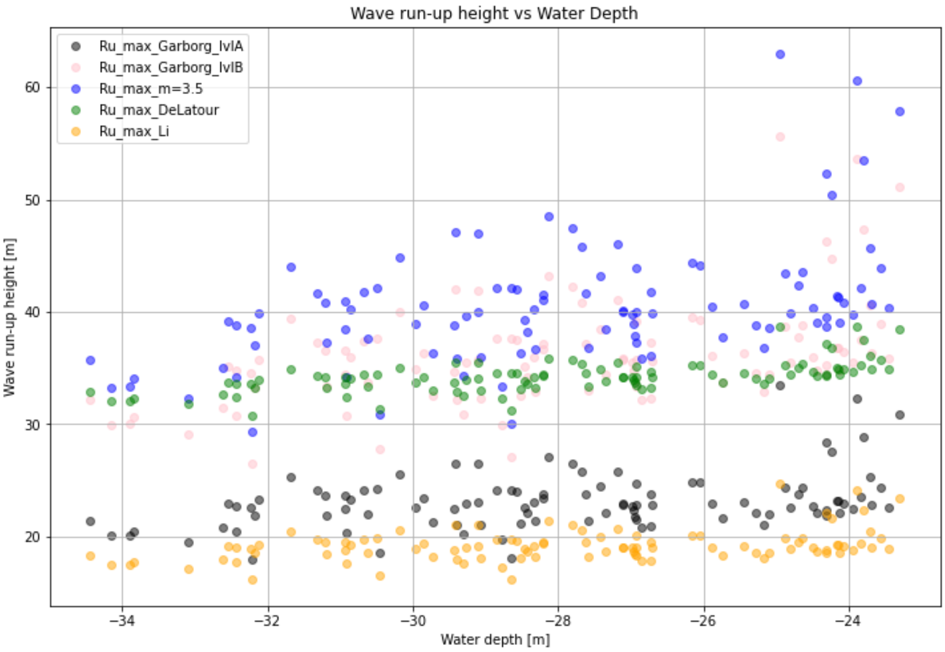

Figure 3.5: Wave run-up height scatter plot for the different methods without any limits.

3.3. Sensitivity study

A sensitivity study of the value m of the method Li is performed since it is the only parameter that is different than three of the four other methods. Instead of m being a single constant value, m depends on wave amplitude $A = \frac{H}{2}$, monopile diameter D, wave number k and radius $a = \frac{D}{2}$. The theory may not hold for the extreme wave heights that are present in the Dogger Bank. Therefore the plots have been created, on the y-axis the m value, on the x-axis the wave height from 2m until 16m. And these have been tested against the wave number and diameter. See figures 3.6 and 3.7

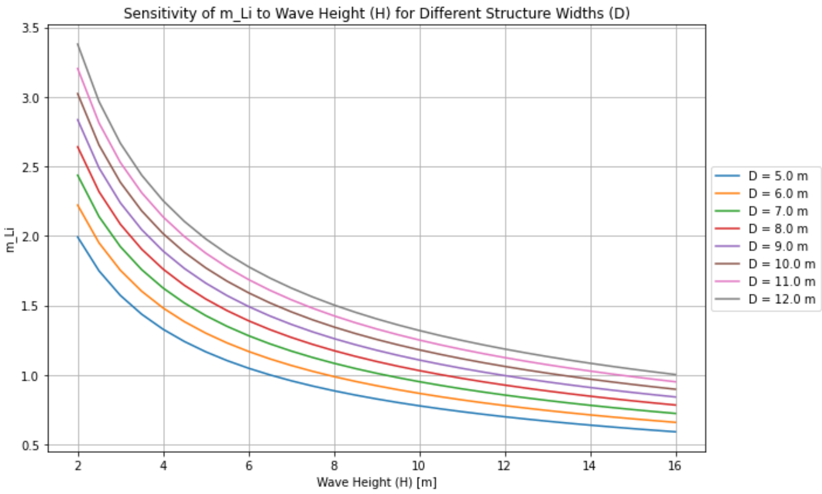

Figure 3.6: m Li vs maximum wave height for different diameters

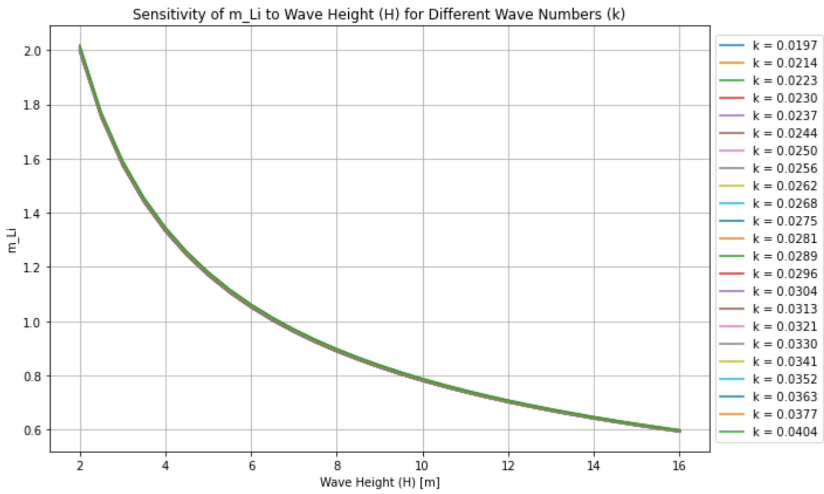

Figure 3.7: m Li vs maximum wave height for different wave numbers

From figure 3.6 it can be concluded that value m depends on both the wave height and the diameter of the monopile. The figure demonstrates a clear trend where m decreases with increasing wave height, particularly for wider structures. And for the larger wave heights the m goes under the value of one as could be expected from figure 3.5.

From figure 3.7 it can be concluded that there is a strong inverse relationship between the wave height and m. But that m is relatively insensitive to the wave number. This means that the wave height is the primary factor influencing m.

3.4. Wave run-up loads

After the wave run-up heights are calculated, the related wave run-up loads can be calculated. This done with following equations:

$$v(z) = \sqrt{2g \cdot (R_u - z)} \tag{3.2}$$

where $v(z)$ is the run-up velocity at the vertical coordinate z [m/s], g the gravitational acceleration $[m/s^2]$, R_u the run-up height [m] and z is the vertical coordinate with respect to the reference level [m].

$$\frac{F}{A} = \frac{1}{2} C_s \rho (v(z))^2 \tag{3.3}$$

where $\frac{F}{A}$ is the load applied on the main access platform [N/m], ρ is the seawater density $[kg/m^3]$, C_s is the slamming coefficient [-] and $v(z)$ is the run-up velocity at the vertical coordinate z [m/s]. The wave run-up loads are calculated for highest wave run-up load for each turbine. When calculating these load the platform is set at 5 different z heights: $z = 10[m]LAT$, $z = 15[m]LAT$, $z = 20[m]LAT$, $z = 25[m]LAT$ and $z = 30[m]LAT$.

A distinction has been made between the local loads and global loads, with $C_{s,global} = 1.5$ and $C_{s,local} = 10$. Andersen and Brorsen, 2007 [19] determined that these are conservatively calibrated slamming coefficients for closed plate platforms.

The local wave run-up loads are defined as the pressure over an area of $0.5m^2$, the middle of this area is taken $2m$ from the monopile edge. The global wave run-up loads are defined as the pressure over the main access platform over an area of $160°$, where the middle is defined as the wave direction. Illustration of both pressure can be found in figures 3.8 and 3.9.

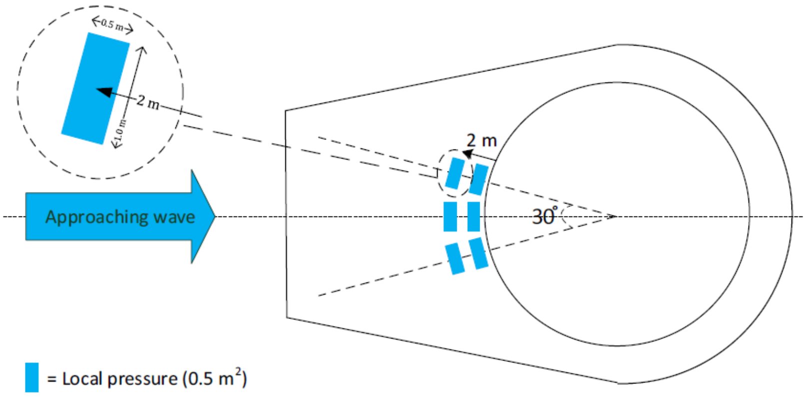

Figure 3.8: Illustration of how the local pressure is applied [?]

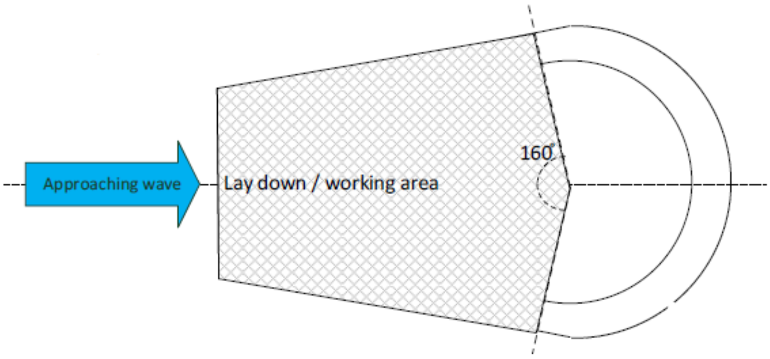

Figure 3.9: Illustration of how the global pressure is apllied [9]

The results of all these calculations are shown in table 3.2 and summarized in figures 3.10 and 3.11. For the simplification of the table only the three highest wave run-up heights and their loads have been calculated. To see if the monopile location is of influence on the wave run-up height, the three highest are documented. It is a possibility that the different methods give a different highest location. In the velocity and loads columns five numbers are shown, these correspond with the reference levels z. The first number corresponds with $z = 30m$ and the last number with $z = 10m$. In the results produced by the method developed by Li [18], some result are given by as 'nan'. In python this means 'not a number', this can be explained for Li because the wave run-up height is not high enough to give a result. If the wave run-up height does not get to the reference height, there will be no velocity and there will be no answer. If there is no water present at the reference height, there can be no loads.

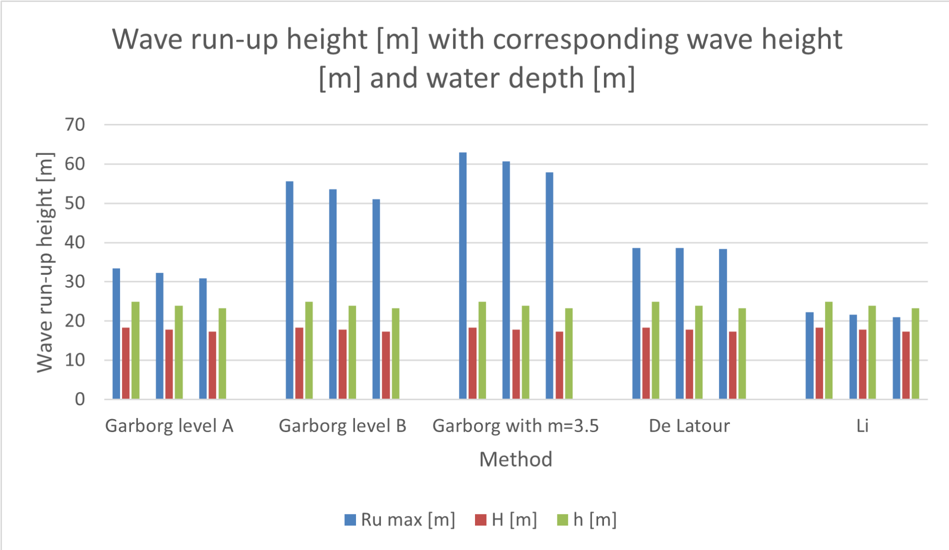

Figure 3.10: Wave run-up height [m] with corresponding wave height [m] and water depth [m]

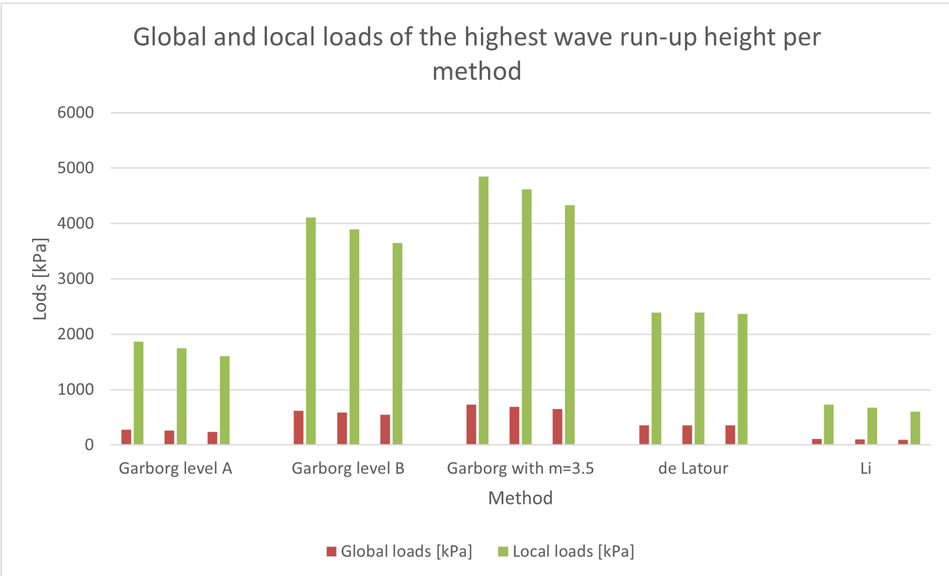

Figure 3.11: Global and local loads of the highest wave run-up heights per method

Table 3.2: Wave run-up height and loads

	Name	h [m]	H [m]	T [s]	u [m/s]	Ru max [m]	z [m]	Vel. in z [m/s]	Global loads [kPa]	Local loads [kPa]
Garborg level A										
	A04	24.95	18.33	11.4	17.2	33.48	30	12.9	128	857
							25	16.26	204	1362
							20	19.04	280	1867
							15	21.47	355	2372
							10	23.64	431	2878
	A01	23.88	17.76	11.4	16.7	32.26	30	11.94	110	733
							25	15.51	185	1238
							20	18.4	261	1744
							15	20.9	337	2249
							10	23.13	413	2754
	B01	23.3	17.36	11.4	16.3	30.88	30	10.74	89	594
							25	14.61	164	1099
							20	17.65	240	1604
							15	20.24	316	2109
							10	22.53	392	2614
Garborg level B										
	A04	24.95	18.33	11.4	17.2	55.63	30	24.52	464	3095
							25	26.44	540	3600
							20	28.23	615	4105
							15	29.92	691	4610
							10	31.52	767	5116
	A01	23.88	17.76	11.4	16.7	53.57	30	23.68	433	2886
							25	25.66	508	3392
							20	27.51	584	3897
							15	29.24	660	4402
							10	30.87	736	4907
	B01	23.3	17.36	11.4	16.3	51.11	30	22.63	395	2638
							25	24.71	471	3143
							20	26.62	547	3648
							15	28.4	623	4154
							10	30.08	698	4659
m=3.5										
	A04	24.95	18.33	11.4	17.2	63.02	30	27.31	576	3841
							25	29.05	651	4346
							20	30.69	727	4851
							15	32.25	803	5356
							10	33.74	879	5862
	A01	23.88	17.76	11.4	16.7	60.67	30	26.46	540	3604
							25	28.25	616	4109
							20	29.94	692	4614
							15	31.53	768	5120
							10	33.05	843	5625
	B01	23.3	17.36	11.4	16.3	57.86	30	25.39	497	3319
							25	27.25	573	3825
							20	29.0	649	4330
							15	30.64	725	4835
							10	32.2	801	5340
de Latour										
	A04	24.95	18.33	17.9	12.3	38.68	30	16.38	207	1381
							25	19.14	283	1887
							20	21.55	358	2392
							15	23.72	434	2897
							10	25.7	510	3402
	A01	23.88	17.76	17.9	12.1	38.64	30	16.36	206	1378
							25	19.12	282	1883
							20	21.54	358	2388
							15	23.71	434	2894
							10	25.69	509	3399
	B01	23.3	17.36	17.9	11.9	38.4	30	16.21	203	1353
							25	19.0	278	1859
							20	21.43	354	2364
							15	23.6	430	2869
							10	25.6	506	3374
Li										
	A04	24.95	18.33	11.4	17.2	22.25	30	nan	nan	nan
							25	6.64	34	227
							20	11.93	109	732
							15	15.5	185	1237
							10	18.4	261	1743
	A01	23.88	17.76	11.4	16.7	21.65	30	nan	nan	nan
							25	5.7	25	167
							20	11.43	100	672
							15	15.12	176	1177
							10	18.08	252	1682
	B01	23.3	17.36	11.4	16.3	20.95	30	nan	nan	nan
							25	4.31	14	95
							20	10.8	90	601
							15	14.66	165	1106
							10	17.69	241	1611

3.5. First conclusion

First of all, regardless of which method is used, the same wind turbine location gives the highest wave run-up height. Since only one method for calculating wave run-up loads is available, these turbines will also experience the highest wave run-up loads.

Secondly, table 3.2 shows that the method from de Latour has the highest wave run-up height and loads for $T = 17.9s$. While the other methods get the highest loads for $T = 11.4s$. The different methods give different results and will therefore be investigated in the numerical model.

It can also be concluded that there is a significant variation in wave run-up heights and therefore a large variation in wave run-up loads. This makes it clear that other methods need to be considered during this process as well to make a better estimation.

The high wave run-up heights and loads are mainly caused by the high particle velocity. This value is squared in the run-up calculation, as seen in table 3.1.

As mentioned before, the wave that gives highest run-up height is the same for all methods. Since this wave gives high values, a closer look is give to the wave. In figures 3.12 and 3.13 the particle velocity and surface elevation of this wave is plotted for all orders N of the stream function. For this model, Fenton's stream function is used [11]. Higher orders of the stream function are not available since the wave theory does not give solutions for them. As can be seen in the figures the solutions vary a lot and do not give a credible solution. The wave is also plotted (blue dot with number 1) in the figure provided by the DNV guidelines, figure 3.14. It can be seen than the wave has a higher H/h ratio that the wave breaking line. Meaning that for this wave, the wave theory does not apply.

Therefore, in the next section possible limitations of the wave run-up height models are discussed to see how to deal with waves like this.

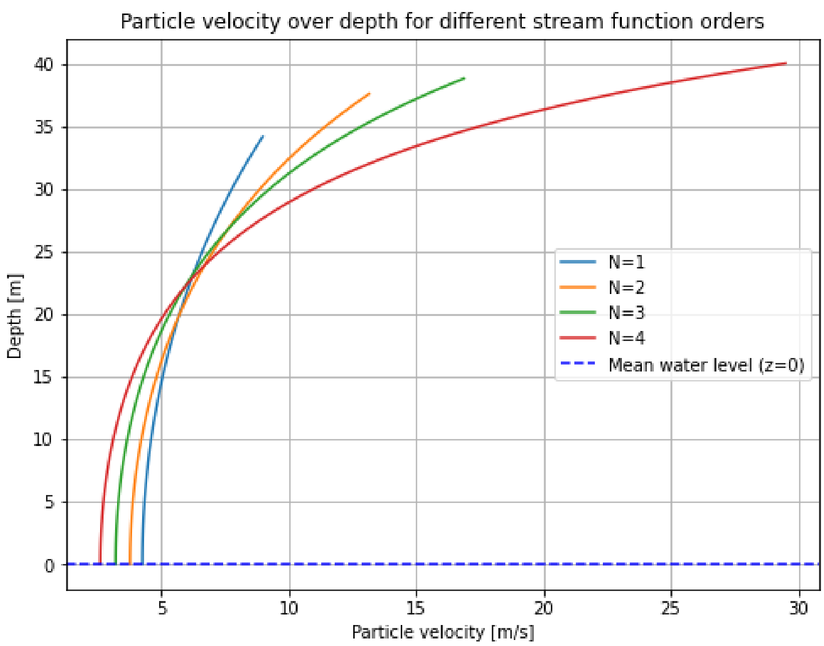

Figure 3.12: Particle velocity for different stream function orders, H=18.3m, T=11.4s and h=24.95m.

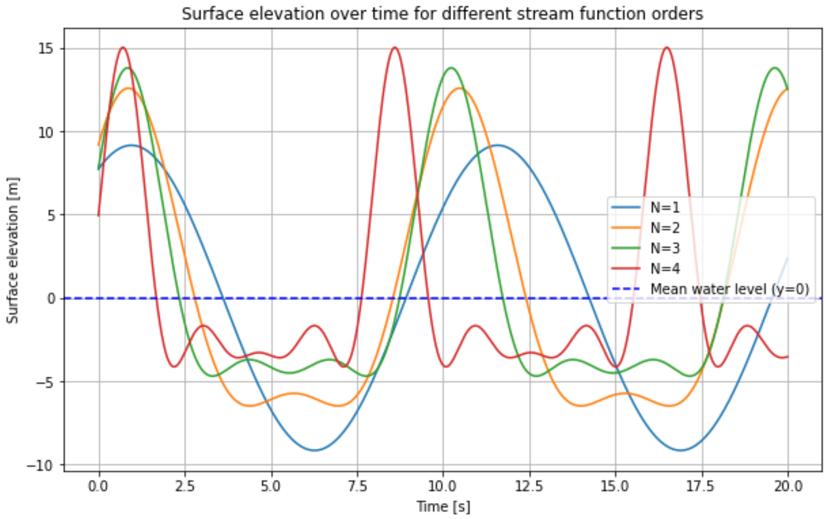

Figure 3.13: Surface elevation for different stream function orders, H=18.3m, T=11.4s and h=24.95m.

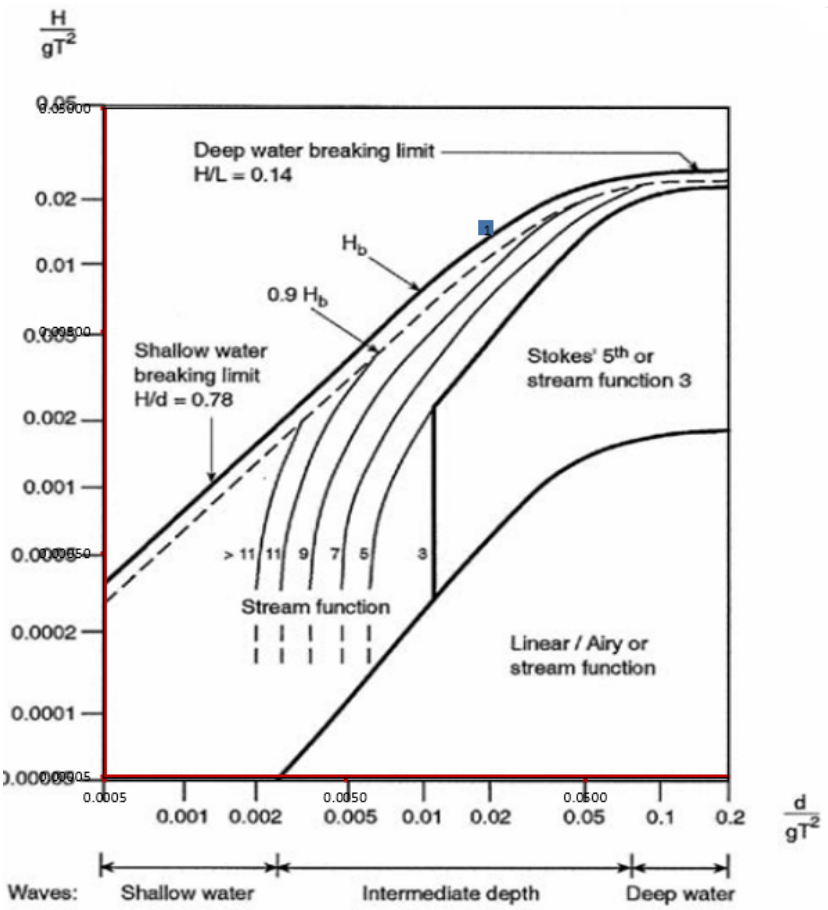

Figure 3.14: DNV guideline, blue dot: H=18.3m, T=11.4s and h=24.95m

4

Limitations and reliability of the analytical models

4.1. Limitations of the wave run-up height models

In this section the basic principles and limitations of the models used in this chapter are discussed.

4.1.1. Wave energy

The presence of a wave at the water surface implies that water particles were moved from their position at rest to a new position. This shift calls for work to move the particles against gravity, in other words it requires potential energy. Besides, the water particles in the wave also move, this movement represents the kinetic energy. To estimate the potential energy, consider a slice of water with thickness Δz in a column with horizontal surface area $\Delta x\ \Delta y$ (see figure 4.1).

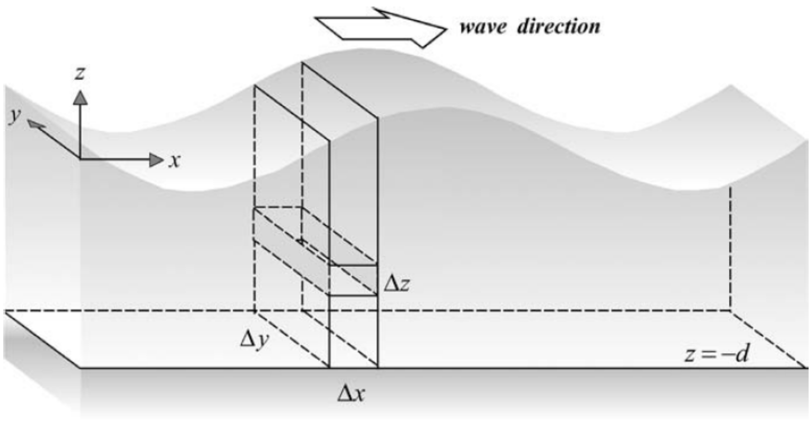

Figure 4.1: The column in the harmonic wave that is used in deriving the expressions for wave energy. [15]

The wave-induced potential energy in the entire water column, from bottom to surface, is equal to the potential energy in the presence of the wave minus the potential energy in absence of the wave [15]. When divided by the horizontal surface area of the column and time-averaged over one period, this gives:

$$E_{\text{potential}} = \overline{\int_{-\mathrm{d}}^{\eta} \rho g z \ \mathrm{d}z} - \overline{\int_{-d}^{0} \rho g z \ \mathrm{d}z} = \overline{\int_{0}^{\eta} \rho g z \ \mathrm{d}z} \tag{4.1}$$

where ρ represents the water density, g the gravitational acceleration and the overbar the time-averaging. For a wave with amplitude a, the outcome of the integral is as follows:

$$E_{\text{potential}} = \overline{\frac{1}{2}\rho g \eta^2} = \frac{1}{4}\rho g a^2 \tag{4.2}$$

The kinetic energy in the same slice of water as above is $\frac{1}{2}\rho \Delta x \Delta y u^2$. This gives the following time-averaged kinetic energy in the entire column:

$$E_{\text{kinetic}} = \overline{\int_{-d}^{\eta} \frac{1}{2}\rho u^2 \, dz} \tag{4.3}$$

The result of this integral using linear theory is:

$$E_{\text{kinetic}} = \frac{1}{4}\rho g a^2 \tag{4.4}$$

The total time-average wave-induce energy density $E = E_{\text{potential}} + E_{\text{kinetic}}$ is then:

$$E = \frac{1}{2}\rho g a^2 \tag{4.5}$$

4.1.2. Origin formula wave run-up height

Most of the analytical models used in this research use the following equation to calculate the wave run-up height on a cylinder:

$$R_u = \eta_{max} + m \cdot \frac{u^2}{2g} \tag{4.6}$$

The first notable experimental work on wave run-up on cylinders was done by Hallermeier, 1976 [14]. In his study on thin circular vertical piles (with diameter $2a$ very much less than a wavelength, L), he suggested that the wave run-up height can be expressed by the velocity head, $\frac{u^2}{2g}$. The assumption is that the water particles are forced to convert their kinetic energy into potential energy, the derivation will be given below and is visualized in figure 4.2.

$$E_{\text{kin}} = E_{\text{pot}} \tag{4.7}$$

$$\frac{1}{2}\rho u^2 = \rho g \Delta z \tag{4.8}$$

This results in the following change in height of the water particle:

$$\Delta z = \frac{u^2}{2g} \tag{4.9}$$

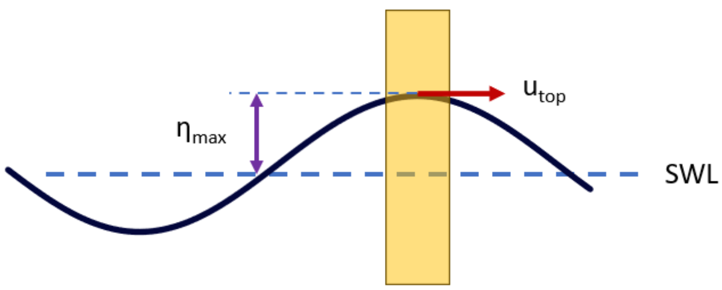

Figure 4.2: Visualization derivation run-up height on a cylinder

This total wave run-up height is the combination of surface elevation and change in height of the water particle:

$$R_u = \eta_{max} + \frac{u^2}{2g} \tag{4.10}$$

where R_u is the run-up height on the vertical cylinder $[m]$, η_{max} the maximum wave crest elevation $[m]$, u^2 the horizontal water particle velocity $[m/s]$ and g the gravitational acceleration $[m/s^2]$. In

1992 Niedzwecki and Duggal [21] performed small scale experiment to investigate the wave run-up on cylinders and found that the wave run-up height in formula 4.10 underestimates the wave run-up height. And therefore added the wave run-up coefficient m, as in formula 4.6. This underestimation of the wave run-up height could be caused by the fact that the amount of energy in the wave is not well represented in this velocity head theory.

4.1.3. Wave against a wall

In this research the wave run-up height on a cylinder is an important parameter. One could argue that the wave run-up height against a cylinder cannot be higher than the wave run-up on a wall since water particles and therefore energy is lost around the cylinder. In figure 4.3 the result of a standing wave is shown. When a regular wave component meets a vertical wall perpendicular to its propagation direction, it is reflected and sent back where it came from with an identical amplitude and speed. The incoming and reflected wave interfere and superimpose. At that point the wave seems to be stationary in space with twice the amplitude of the incoming wave. In a case of 100% reflection $a_i = a_r$, the surface elevation is as follows:

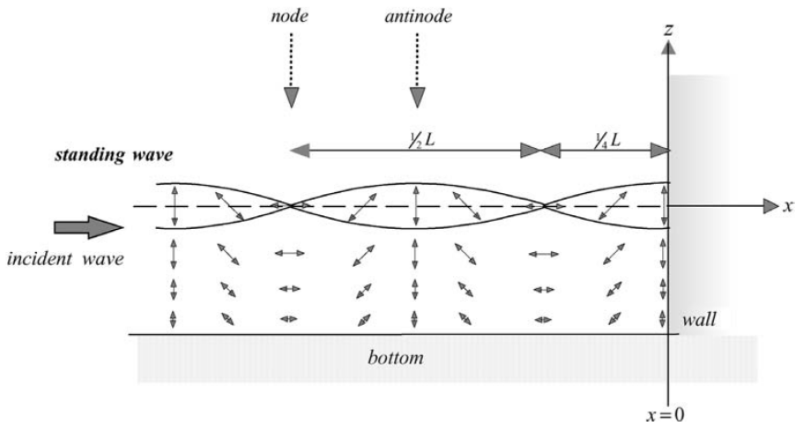

Figure 4.3: A standing wave due to the full reflection of an incident wave against a vertical wall. The short straight arrows are the trajectories of the water particles as they undergo their motion in one wave period. [15]

$$\eta(x,t) = 2a_i \cos(kx)\sin(\omega t) \tag{4.11}$$

The surface elevation of this standing wave fluctuates as a sine wave in time. The maximum run-up on a wall at $x = 0$ can therefore be written as:

$$R_u = 2a_i \tag{4.12}$$

Ning et al., 2017 [22] found that the peak free surface elevation on a wall is approximately 2.6 times the incoming wave amplitude.

$$R_u = 2.6a_i \tag{4.13}$$

This exceeds the result of the perfect reflection discussed above. The possible reason for this is the non-linear interaction of the incoming wave groups with the vertical wall. This approximation for the maximum wave run-up on a wall will be considered in this research.

In the EurOtop manual [27] in section 5.2.4, it is stated that the wave run-up limit for a vertical wall is the following:

$$Ru = 1.8H_{m0} \tag{4.14}$$

The EurOtop manual is a guideline on the prediction of wave overtopping for coastal structures. There is also a section for wave run-up on vertical walls in intermediate water.

All 3 of these limits will be presented later in the study to see if they can be implemented as a high limit for wave run-up on monopiles.

4.1.4. Limitations of the experiments used in the development of the different wave run-up equations

In this section the limitations of the experiments used in the development of the different wave run-up equations as given in Table 3.1 are explained. When developing these equations, the researchers relied on experiments performed in small- and large-scale wave tanks. Therefore it is useful to look into the boundaries of these experiments. Then it is known when it is possible to use them and when they are outside the boundaries of the experiments. A common quick estimation of the steepness of the wave is the dimensionless parameter H/h. These values of the methods used in this research are shown in table 4.1.

Table 4.1 shows that the high limit in which the methods have been tested are: 0.37, 0.46 and 0.4. Garborg et al., 2020 [12] used the experiments performed by Andersen et al., 2011 [20]. In their experiments, they tried to make waves with a H/h ratio higher than 0.46, but did not succeed. It was impossible for them to generate waves with a ratio of 0.5 because of the flat bottom configuration. This was due to waves breaking just in front of the wave paddle. Since the waves in the wind farm analyzed in this research are also on a relatively flat bottom, this H/h ratio might be something to keep in mind as a potential limit of the waves analyzed.

Table 4.1: H/h values of the different methods

	H/h	**Remark**
Garborg	0.35-0.46	Tried for higher wave heights, but waves would break immediately.
Garborg with m=3.5	0.35-0.46	
de Latour	0.27-0.37	
Li	0.23-0.40	

4.1.5. Lowering the wave height to reach wave length convergence

Another method to make sure the waves are in the range of the stream function, is to lower the wave height until wave length convergence is reached for the higher orders of the stream function. The goals of this wave length convergence is to make sure that parameters, as particle velocity of the wave over depth and the surface elevation of the wave do not vary when using different stream function orders.

4.2. Wave run-up heights and loads with limits

In this section two different methods are discussed to get more realistic wave run-up height results and to eliminate unrealistic waves. The first one is: implementing the H/h limit from the experiments. The second one is: lowering the wave height until wave length convergence in the higher orders of the stream function is reached.

4.2.1. Implementing an H/h limit

In this section a fixed H/h limit is implemented, this H/h is 0.46 and is the high limit of the experiments from Garborg et al., 2019 [12]. All wave heights in this section are lowered since the water depth per location is fixed and the H/h is fixed as well. In figure 4.4 the wave run-up heights are plotted. The figure shows that for all methods the wave run-up height declines more or less linear for a declining water depth. A difference with the method without limit is that the method of de Latour now becomes the method with the highest wave run-up. A possible explanation for this is that the particle velocity of the wave is not present in the equations, as opposed to the other methods where it is dominant. It is also worth pointing out that with this method the monopile locations with larger water depth give the highest wave run-ups. In the method without this limit it was the locations with the smaller water depths where the highest run-ups where located.

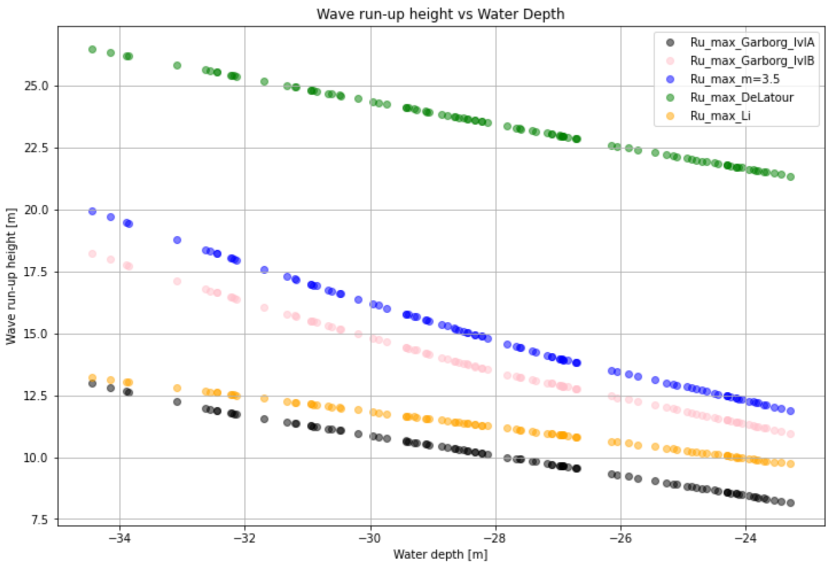

Figure 4.4: Wave run-up heights with H/h limit

In figure 4.5 the location in the DNV guideline figure of the three waves that gives the highest wave run-up are shown. It can be seen in the figure that the waves with this limit are not over, on or close to the boundary of the stream function theory anymore. Due to the fixed H/h limit and the waves having the same wave period, they are all three almost on the same location. The waves within this limit are not close to the theoretical limit of the theory but are on the limit of the small- and large-scale experiments conducted.

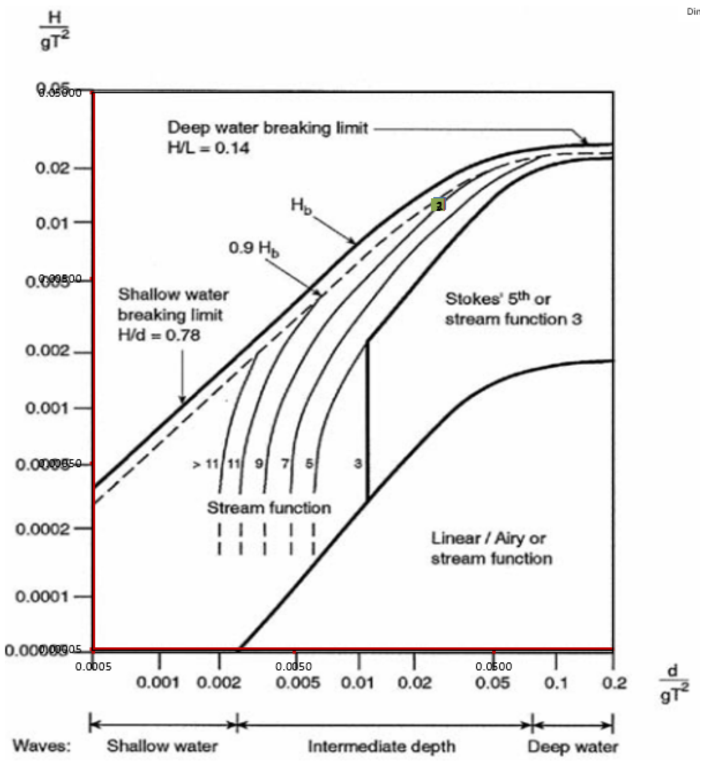

Figure 4.5: Location of the 3 highest wave run-up location from table 4.1 in the DNV guideline. The 3 dots are on top each other because they have same location.

In table 4.2 all relevant information can be found of the monopile locations with the highest run-up for each method. In the last three columns the information refers to the following locations: z heights: $z = 10[m]LAT$, $z = 15[m]LAT$, $z = 20[m]LAT$, $z = 25[m]LAT$ and $z = 30[m]LAT$. The particle velocities of the locations with the highest wave run-up is a lot lower than in the method without limit. Due to this the wave run-up heights are lower. From this also follows that for the for the higher reference locations no answer is found.

In figure 4.6 the wave run-up height for each method with corresponding wave height and water depth can be found. It can be seen that the highest wave run-up is now for the locations with the greatest water depth.

Figure 4.6: Wave run-up height [m] for H/h =0.46 with corresponding wave height [m] and water depth [m]

Table 4.2: Wave run-up height and loads with H/h limit, three highest wave run-up results per method from Figure 4.4

	Name	h [m]	H [m]	T [s]	u [m/s]	Ru max [m]	z [m]	Vel. in z [m/s]	Global loads [kPa]	Local loads [kPa]
Garborg level A										
							30	nan	nan	nan
							25	nan	nan	nan
	A10	34.44	15.84	11.40	8.31	13.06	20	nan	nan	nan
							15	nan	nan	nan
							10	7.74	46	308
							30	nan	nan	nan
							25	nan	nan	nan
	H15	34.15	15.71	11.40	8.25	12.89	20	nan	nan	nan
							15	nan	nan	nan
							10	7.53	43	292
							30	nan	nan	nan
							25	nan	nan	nan
	A08	33.89	15.59	11.40	8.19	12.75	20	nan	nan	nan
							15	nan	nan	nan
							10	7.34	41	277
Garborg level B										
							30	nan	nan	nan
							25	nan	nan	nan
	A10	34.44	15.84	11.40	8.31	18.33	20	nan	nan	nan
							15	8.09	50	336
							10	12.79	126	842
							30	nan	nan	nan
							25	nan	nan	nan
	H15	34.15	15.71	11.40	8.25	18.09	20	nan	nan	nan
							15	7.79	46	312
							10	12.60	122	817
							30	nan	nan	nan
							25	nan	nan	nan
	A08	33.89	15.59	11.40	8.19	17.88	20	nan	nan	nan
							15	7.52	43	290
							10	12.43	119	796
m=3.5										
							30	nan	nan	nan
							25	nan	nan	nan
	A10	34.44	15.84	11.40	8.31	20.09	20	1.36	1	9
							15	10.00	77	514
							10	14.07	152	1019
							30	nan	nan	nan
							25	nan	nan	nan
	H15	34.15	15.71	11.40	8.25	19.83	20	nan	nan	nan
							15	9.73	73	487
							10	13.89	148	992
							30	nan	nan	nan
							25	nan	nan	nan
	A08	33.89	15.59	11.40	8.19	19.59	20	nan	nan	nan
							15	9.49	69	463
							10	13.72	145	969
de Latour										
							30	nan	nan	nan
							25	nan	nan	nan
	A10	34.44	15.84	11.40	8.31	20.23	20	1.43	2	10
							15	10.08	79	523
							10	14.19	154	1035
							30	nan	nan	nan
							25	nan	nan	nan
	H15	34.15	15.71	11.40	8.25	19.98	20	nan	nan	nan
							15	9.81	75	500
							10	14.02	150	1002
							30	nan	nan	nan
							25	nan	nan	nan
	A08	33.89	15.59	11.40	8.19	19.75	20	nan	nan	nan
							15	9.56	71	474
							10	13.85	147	978
Li										
							30	nan	nan	nan
							25	nan	nan	nan
	A10	34.44	15.84	11.40	8.31	20.92	20	2.03	4	19
							15	10.46	85	563
							10	14.77	163	1106
							30	nan	nan	nan
							25	nan	nan	nan
	H15	34.15	15.71	11.40	8.25	20.64	20	nan	nan	nan
							15	10.24	80	530
							10	14.59	159	1077
							30	nan	nan	nan
							25	nan	nan	nan
	A08	33.89	15.59	11.40	8.19	20.37	20	nan	nan	nan
							15	9.97	76	500
							10	14.41	156	1048

4.2.2. Lowering the wave height to reach wave length convergence

In this section another limit is used to search for waves within the boundaries of the stream wave function and with wave length convergence over the stream function orders. To ensure this correct solution for the wave is reached, the surface elevations of the wave should not include any non-linearities, second peaks for example. The particle velocities over depth should hardly have any difference for different stream function orders. When this goal is reached, the goal of a mathematically sound wave solution is achieved, and we do not have a numerical solution which cannot exist. For this section the three highest wave run-up locations for the method without limit is used (table 3.2).

First the wave height is lowered from $18.4m$ to $H = 16.5m$, while the water depth stays $24.95m$ and the wave period stays $11.4s$. At this wave height we do get solutions for all orders of the stream function. The DNV guideline, wave length over N, particle velocity and surface elevation are plotted below. The DNV guideline, figure 4.11 shows that the wave is just within the theoretical boundary of the stream function. But the other three figures show that the wave does not get consistent results for all the order of the stream function. This means this wave cannot be used and the wave height is still too high.

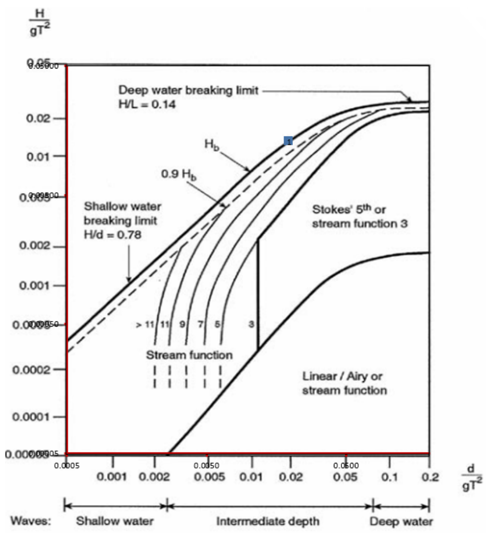

Figure 4.7: The blue dot represents the lowered wave height: H=16.5m in the DNV guideline

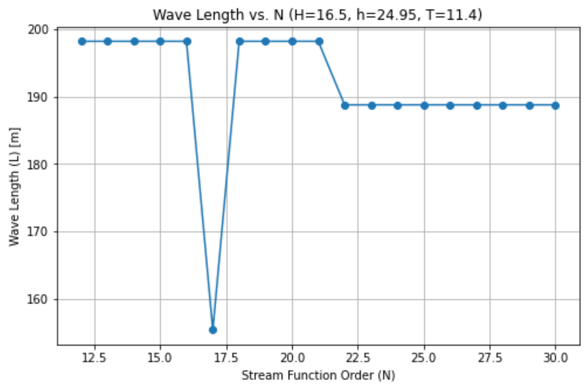

Figure 4.8: H=16.5m wavelength over N

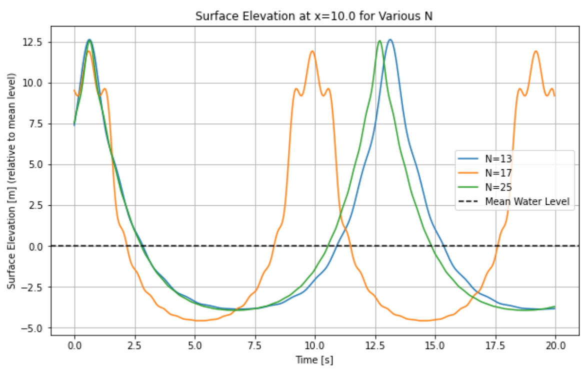

Figure 4.9: H=16.5m, surface elevation

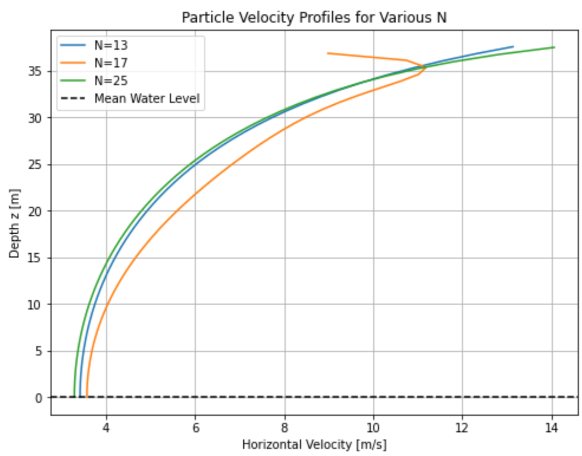

Figure 4.10: H=16.5m, particle velocity

The process of lowering the wave height is repeated until a result with wave length convergence is achieved. In this case the wave height had to be lowered until $H = 15.9m$. The results are shown below:

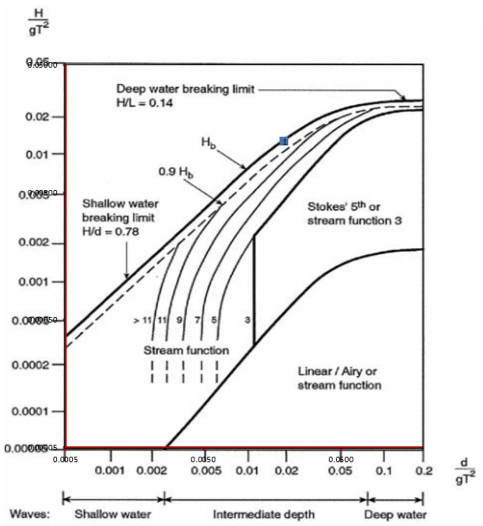

Figure 4.11: H=15.9m DNV guideline

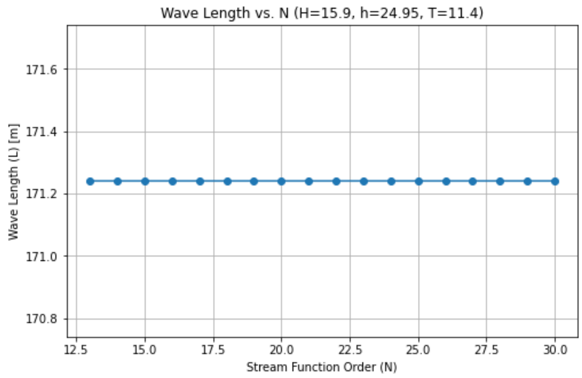

Figure 4.12: H=15.9m wavelength over N

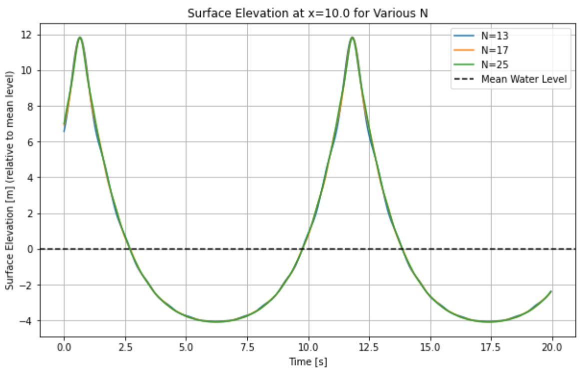

Figure 4.13: H=15.9m, surface elevation

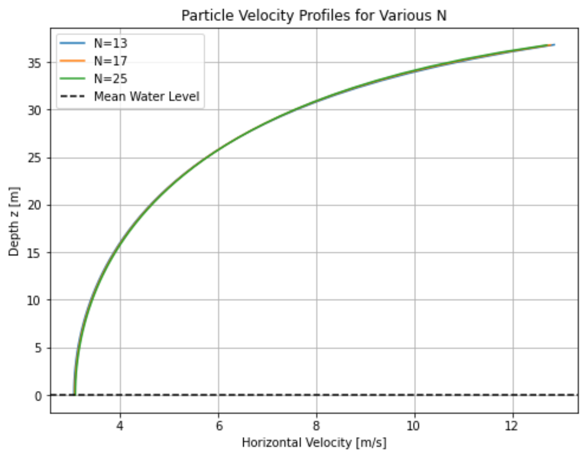

Figure 4.14: H=15.9m, particle velocity

For the wave with the highest wave run-up the wave height had to be lowered from 18.5m to 15.9m for this limit. The process is repeated for the other two waves as well. The results of this limit can be found in table 4.3. The wave run-up height with their corresponding wave height and water depth is shown in figure 4.15. The wave run-up height results are higher than for the H/h over limit but lower than for the one without limit.

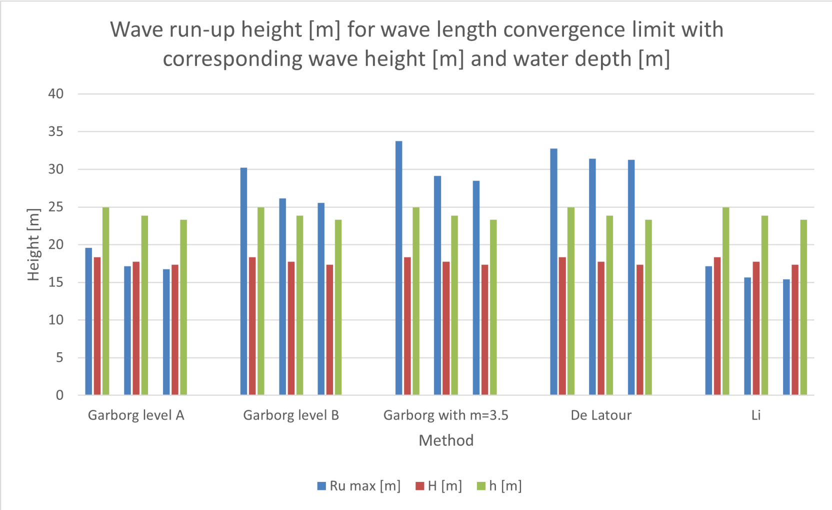

Figure 4.15: Wave run-up height [m] for wave length convergence limit with corresponding wave height [m] and water depth [m]

Table 4.3: Wave run-up height and loads with wave length convergence limit

	Name	h [m]	H [m]	T [s]	u [m/s]	Ru max [m]	z [m]	Vel. in z [m/s]	Global loads [kPa]	Local loads [kPa]
Garborg level A										
							30	nan	nan	nan
							25	nan	nan	nan
	A04	24.95	15.90	11.4	12.7	19.56	20	nan	nan	nan
							15	9.46	69	460
							10	13.69	144	965
							30	nan	nan	nan
							25	nan	nan	nan
	A01	23.88	14.90	11.4	12.2	17.13	20	nan	nan	nan
							15	6.47	32	215
							10	11.83	108	720
							30	nan	nan	nan
							25	nan	nan	nan
	B01	23.30	14.60	11.4	12.1	16.74	20	nan	nan	nan
							15	5.84	26	175
							10	11.50	102	680
Garborg level B										
							30	1.97	3	20
							25	10.10	78	525
	A04	24.95	15.90	11.4	12.7	30.20	20	14.15	154	1030
							15	17.27	230	1535
							10	19.91	306	2040
							30	nan	nan	nan
							25	4.71	17	114
	A01	23.88	14.90	11.4	12.2	26.13	20	10.97	92	619
							15	14.78	168	1124
							10	17.79	244	1629
							30	nan	nan	nan
							25	3.21	7	53
	B01	23.30	14.60	11.4	12.1	25.53	20	10.41	83	558
							15	14.37	159	1063
							10	17.45	235	1568
m=3.5										
							30	8.57	56	378
							25	13.10	132	883
	A04	24.95	15.90	11.4	12.7	33.74	20	16.42	208	1388
							15	19.18	284	1894
							10	21.58	359	2399
							30	nan	nan	nan
							25	9.00	62	416
	A01	23.88	14.90	11.4	12.2	29.13	20	13.38	138	922
							15	16.65	214	1427
							10	19.37	289	1932
							30	nan	nan	nan
							25	8.23	52	349
	B01	23.30	14.60	11.4	12.1	28.46	20	12.88	128	854
							15	16.25	203	1359
							10	19.03	279	1864
de Latour										
							30	7.35	41	278
							25	12.33	117	783
	A04	24.95	15.90	17.9	10.7	32.75	20	15.82	193	1288
							15	18.66	269	1793
							10	21.13	344	2298
							30	5.24	21	141
							25	11.20	96	646
	A01	23.88	14.90	17.9	10.0	31.40	20	14.95	172	1151
							15	17.94	248	1656
							10	20.49	324	2162
							30	4.99	19	128
							25	11.09	95	633
	B01	23.30	14.60	17.9	9.9	31.27	20	14.87	170	1138
							15	17.87	246	1643
							10	20.43	322	2149
Li										
							30	nan	nan	nan
							25	nan	nan	nan
	A04	24.95	15.90	11.4	12.7	17.12	20	nan	nan	nan
							15	6.44	32	213
							10	11.82	107	718
							30	nan	nan	nan
							25	nan	nan	nan
	A01	23.88	14.90	11.4	12.2	15.65	20	nan	nan	nan
							15	3.56	9	65
							10	10.53	85	570
							30	nan	nan	nan
							25	nan	nan	nan
	B01	23.30	14.60	11.4	12.1	15.40	20	nan	nan	nan
							15	2.81	6	40
							10	10.3	81	545

4.3. Reliability

In this chapter it can be seen that the reliability of the analytical models can be come an issue when the H/h ratio of the waves becomes extreme. When working with extreme waves it is important to take a closer look at the limits of the wave run-up models. The extreme waves in this research have H/h ratios beyond the scope of the experiments used to validate the wave run-up models with. Therefore, there is need for limits to make sure the wave run-up results get more reliable.

The $H/h = 0.46$ limit of the experiments of Garborg et al., 2020 [12] is plotted in figure 4.16. The location of the highest wave is shown in the graph as the dot. It is found that none of the Dogger Bank locations are on or within the $H/h = 0.46$ limit of the experiments performed. This highest location has a H/h ratio of 0.74 and the location with the lowest H/h ratio is 0.57. This means all of the locations are calculated outside of the range where these models are calibrated with, and the reliability of the results goes down.

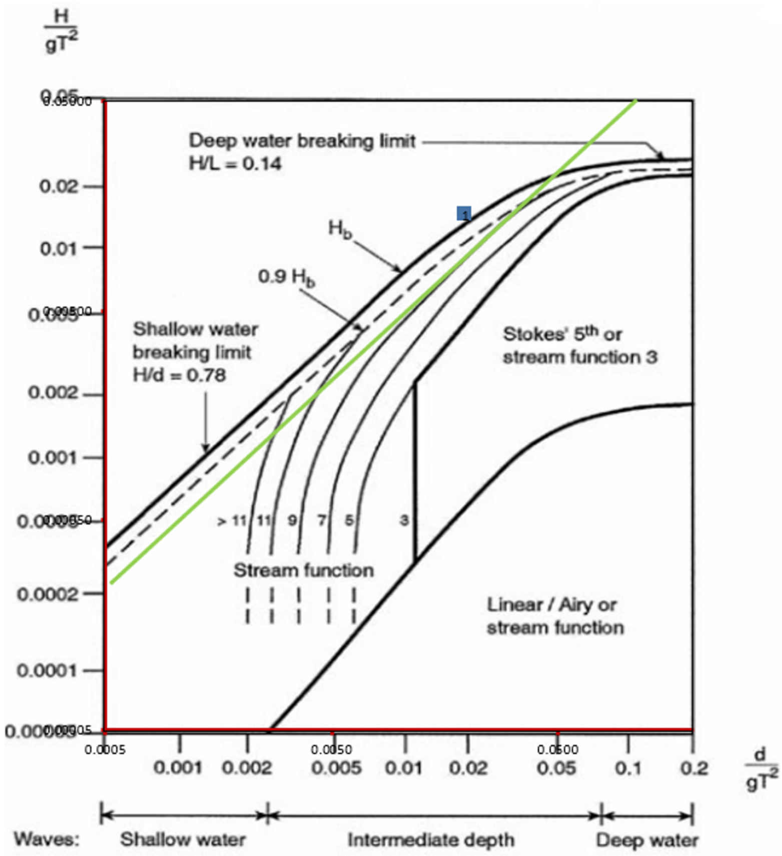

Figure 4.16: DNV guideline [8] with H/h limit of experiments used in Garborg et al., 2020 [12]

In chapter 6 a 2-dimensional numerical is introduced to investigate if this can be used as such a limit.

4.4. Conclusion

In this chapter the wave run-up heights and loads are calculated without a limit, a limit based on small- and large-scale experiments and a limit based on wave length convergence to get more realistic waves within the stream function theory. A summary of the wave run-up height results is given in table **??**. The following conclusions can be drawn

- When calculating with wave heights close to breaking wave heights, it must be checked if the waves are within the limits of the wave theory and if the solutions are stable.

- It has been observed that the application of the wave run-up height models can lead to very high wave run-up heights. Application of stream function theory, without checking for wave length convergence, can results in high orbital velocities and therefore high wave run-up heights. This could be caused because the models are used outside the boundaries where they validated against. They are also beyond the theoretical limit of a standing wave against a wall, which in the case of a wave hitting a cylinder is considered an upper bound.
- The equations that use the wave run-up formulation based on the stagnation head theory are heavily influenced by the particle velocity of the wave. This is the main parameter that drives the wave run-up height since it is squared in the equation.
- The spread in wave run-up height over the model without limit and the model with the two limits is less for the de Latour and Li equations than it is for the other ones.
- When working with steep waves that are close to breaking it is possible that these do not perform very well. The steepness of the waves where the equations are validated with is up to a H/h ratio of 0.46. It was for the researchers not possible to create steeper waves for flat seabeds. This means that the wave run-up heights that are calculated are outside the range where the empirical relations are derived for, and therefore the reliability of the results can be questioned.
- In figure 4.16 the line with the H/h limit is drawn and is concluded that without any limit all Dogger Bank locations are above this line and are used outside the scope of the models. Therefore the results are less reliable without any limits.
- The highest three methods in the wave convergence limit have wave run-up heights that are approximately 2 times the maximum wave height. These wave run-up heights are still higher than the theoretical wave run-up on a wall of $2.6a_i$, which is considered not possible.
- It can be observed that the method of Li gives the lowest wave run-up height. The difference between Li and the other method is that Li uses regular wave experiments to calibrate their results while Garborg and de Latour use irregular wave experiments. This could explain the difference between the methods since regular wave do not account for the nonlinearities that occur in irregular wave fields and could therefore underestimate the wave run-up height.

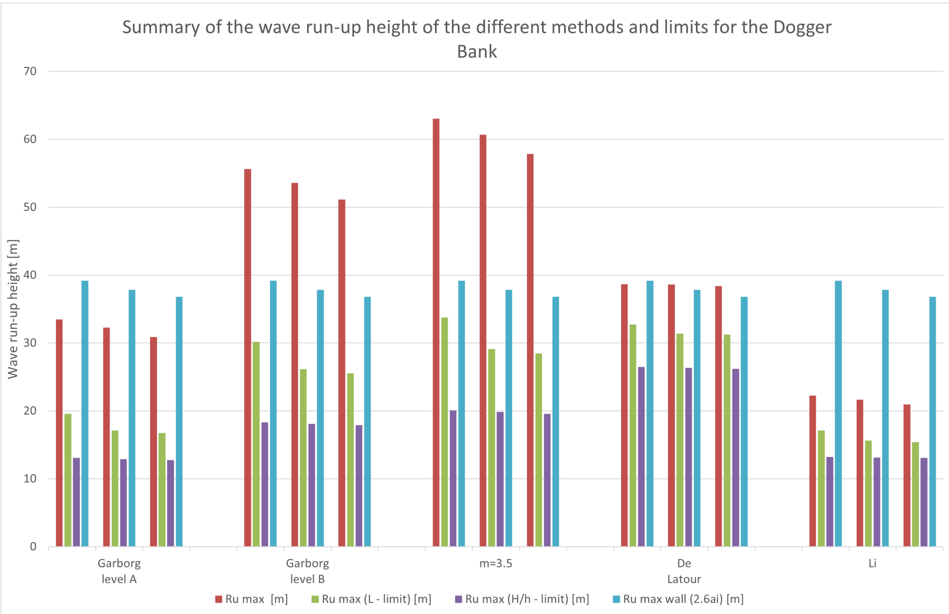

Figure 4.17: Summary of the wave run-up height of the different methods and limits for the Dogger Bank.

Table 4.4: Summary of the wave run-up height of the different methods and limits for the Dogger Bank

	Name	**Ru max [m]**	**Ru max (L - limit) [m]**	**Ru max (H/h - limit) [m]**	**Ru max wall (2.6ai) [m]**
	A04	33.48	19.56	13.06	39.18
Garborg level A	A01	32.26	17.13	12.89	37.83
	B01	30.88	16.74	12.75	36.79
	A04	55.63	30.2	18.33	39.18
Garborg level B	A01	53.57	26.13	18.09	37.83
	B01	51.11	25.53	17.88	36.79
	A04	63.02	33.74	20.09	39.18
Garborg with m=3.5	A01	60.67	29.13	19.83	37.83
	B01	57.86	28.46	19.59	36.79
	A04	38.68	32.75	26.49	39.18
de Latour	A01	38.64	31.4	26.35	37.83
	B01	38.4	31.27	26.22	36.79
	A04	22.25	17.12	13.23	39.18
Li	A01	21.65	15.65	13.14	37.83
	B01	20.95	15.4	13.06	36.79

5

Connection between 2D and 3D wave run-up

This chapter investigates whether a relationship can be found to link 2D and 3D wave run-up heights. The link would be a way to compare the results of the analytical models validated with 3D experiments with the 2D numerical model discussed in the next chapter.

5.1. Theoretical formulas

The linear diffraction theory allows calculation of the wave field around a body of arbitrary shape. The solution for a cylinder is shown in equation 5.1. The wave run-up at chosen angle ($Ru(\theta)$ is the maximum value of the surface elevation η.

$$\frac{\eta}{H} = \mathrm{Re}\left[\left[\sum_{m=0}^{\infty} \frac{i\beta_m \cos(m\theta)}{\pi ka H_m^{(1)'}(ka)}\right] \cdot e^{-i\omega t}\right] \tag{5.1}$$

where $H_m^{(1)'}$ is a Hankel function of the first kind and
$\beta_m = 1$, $m = 0$
$\beta_m = 2(-1)^m i^m$, $m > 0$
$k = 2\pi/L$, wave number
and with the following reference levels:

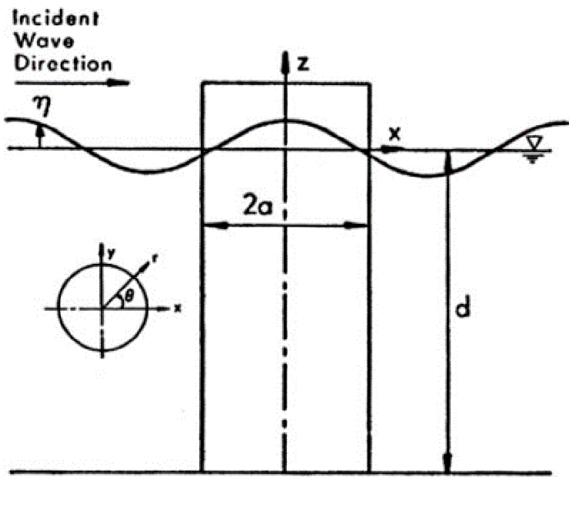

Figure 5.1: Wave diffraction around a cylinder.

It has been tried to extract analytical solutions out of equation 5.1, but it was not possible to generate run-up values.

As no analytical solution for the maximum value of the expression for η exists, an approximation is used [7].

$$\frac{R_\mathrm{u}}{\eta_\mathrm{max}} = \left[1 + \left(\frac{2\pi D}{L}\right)^2\right]^{1/2} \tag{5.2}$$

where η_max is the maximum surface elevation [m], D the diameter of the cylinder [m] and L the wave length [m].

After investigating it seems that these are not equations for wave run-up height but this equation describes the free surface around a cylinder.

5.2. Conclusion

There are at this moment no analytical models to compare 2D and 3D wave run-up results. This could be for further research.

6

2D numerical model

In this chapter, the theoretical formulations of the two numerical models are explained; after this, the difference between the use of 2-dimensional vs. a 3-dimensional model is discussed. Then, the 2-dimensional model is explained, and the results from this model are compared to the analytical wave run-up formulations. The goal is to gain insight into whether a relatively quick numerical model can help to predict the wave run-up height on monopile more accurately.

6.1. Theoretical formulation of the numerical model

In this section, some theoretical background will be provided on the two numerical models used to solve the problem. The first is OceanWave3D, developed by Engsig-Karup et al., 2009 [10]. The second is waves2Foam from Jacobsen et al., 2012 [16]. OceanWave3D is a fully non-linear potential flow solver using a flexible order finite difference method. Waves2Foam is a package for introducing and sampling free surface waves in the open source CFD toolbox OpenFOAM. Then these two are linked to each other as described in Paulsen et al., 2014 [23]. The final numerical solver is shown in Figure 6.1

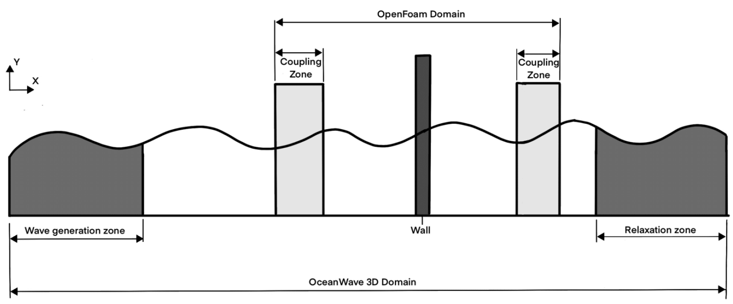

Figure 6.1: Visualization of the coupled numerical model.

6.1.1. OceanWave3D

The numerical solver OceanWave3D is capable of propagating fully nonlinear 3D waves up to the point of breaking. The solver uses a Cartesian coordinate system with the xy-plane located at the still water level and the z-axis pointed upwards. In this study, the solver is used for 2D wave propagation. In the y-direction of the grid a only one cell will be used, making it a 2D problem.

It is assumed that the fluid is inviscid and the flow is irrotational. Assuming 2D the velocity potential relates to the fluid velocities in the following way

$$\mathbf{u} = \nabla \cdot \phi \tag{6.1}$$

with ϕ being the velocity potential, the velocity vector $\mathbf{u}$ and the nabla operator ∇ relate to the horizontal and vertical fluid velocities the following way, Pavilons et al., 2022 [24]

$$\mathbf{u} = (u_x, u_z) \tag{6.2}$$

$$\nabla = \left(\frac{\partial}{\partial x}, \frac{\partial}{\partial z}\right) \tag{6.3}$$

The evolution of the free surface conditions, η, is governed by the kinematic and dynamic free surface conditions. The kinematic free surface condition is described as

$$\frac{\partial \eta}{\partial t} = -\frac{\partial \eta}{\partial x}\frac{\partial \tilde{\phi}}{\partial x} + \frac{\partial \tilde{\phi}}{\partial z}\left(1 + \left(\frac{\partial \eta}{\partial x}\right)^2\right) \tag{6.4}$$

η being the free surface elevation and t the time. The velocity potential at the free surface is described with

$$\tilde{\phi} = \phi\big|_{z=\eta} \tag{6.5}$$

The dynamic free surface condition is given as (Paulsen et al., 2014 [23])

$$\frac{\partial \tilde{\phi}}{\partial t} = -g\eta - \frac{1}{2}\left(\left(\frac{\partial \tilde{\phi}}{\partial x}\right)^2 - \left(\frac{\partial \tilde{\phi}}{\partial z}\right)^2\left(1 + \left(\frac{\partial \eta}{\partial x}\right)^2\right)\right) \tag{6.6}$$

with g the gravitational acceleration.

The full mathematical framework can be found in Engsig-Karup et al., 2009 [10].

6.1.2. Waves2Foam

The wave structure interaction analysis is performed in the OpenFOAM domain with the waves2Foam [16] toolbox.

The governing equations for the combined flow of air and water are given by the Reynolds averaged Navier-Stokes equations

$$\frac{\partial \rho \mathbf{u}}{\partial t} + \nabla \cdot \left[\rho \mathbf{u}\mathbf{u}^T\right] = -\nabla p^* - \mathbf{g} \cdot \mathbf{x}\nabla \rho \quad +\nabla \cdot \left[\mu \nabla \mathbf{u} + \rho \tau\right] + \sigma_T \kappa_\gamma \nabla \gamma \tag{6.7}$$

coupled with the continuity equation for in-compressible flows

$$\nabla \cdot \mathbf{u} = 0 \tag{6.8}$$

Here $\mathbf{u} = (u, v, w)$ is the velocity vector field in Cartesian coordinates, p^* is the pressure in excess of the hydrostatic, ρ is the density, $\mathbf{g}$ is the gravitational acceleration and μ is the dynamic molecular viscosity.

Since the analysis is performed in 2D instead of 3D, the y-directions are neglected and equation 6.7 becomes

$$\frac{\partial \rho \mathbf{u}}{\partial t} + \nabla \cdot (\rho \mathbf{u})\mathbf{u}^T = \nabla p^* - (\mathbf{g} \cdot \mathbf{x})\nabla \rho \tag{6.9}$$

$\mathbf{u}$ and $\mathbf{x}$ are the fluid velocity and position vectors.

The full mathematical description can be found in Jacobsen et al., 2012 [16]

One of the most commonly used ways to capture free-surface flow in OpenFOAM is via the volume of Fluid (VOF) approach. This tracks the interface by solving for a phase friction field α. Jacobsen et al. 2012 [16] implemented this VOF method in their waves2foam solver.

$$\frac{\partial \alpha}{\partial t} + \nabla \cdot \mathbf{u}\alpha + \nabla \cdot u_r \alpha (1 - \alpha) = 0 \tag{6.10}$$

Where u_r is a relative velocity. The fluids are tracked by a scalar field α. α is 0 for air and 1 for water, and any intermediate value is a mixture of the two fluids.

6.2. Shortcomings 2D numerical model

The goal of this research is to investigate whether a simple and time-efficient numerical model can be used to calculate wave run-up height and loads. This means a 2-dimensional model needs to be used because a 3-dimensional model is not time efficient, the calculations time will take 2-3 weeks and is therefore out of the question. A 2-dimensional model, however, comes with some drawbacks.

In table 6.1 a summary of the differences between a 2-dimensional and 3-dimensional numerical is provided.

Table 6.1: Comparison of a 2D vs a 3D numerical model

Aspect	**2D model**	**3D model**
Computational cost	Approx. 3 hours	2/3 weeks
Structure	(Too) simple, no possibility for water to flow around.	Realistic but complex
Wave propagation	One direction only	Multidirectional is a possibility (not necessary in this case)
Wave run-up loads	Possible overestimation due to water not being able to leave	More accurate analysis of the loads
Usage	Initial design phase	Final design phase

A 2D model of a monopile means that it becomes a model that calculates waves against a wall since no water can go through because of the lack of a third dimension. It is assumed in this study that wave run-up on monopile can be never be higher than wave run-up on a monopile. The reasoning behind this is that a monopile is 3D structure, this means that when there is wave run-up not all wave energy will go in vertical direction. Energy will also spread around the structure in horizontal direction. If we compare this with a wall, there will be less wave energy available to go in the vertical direction. This will lead to less wave run-up. Since it is theoretically impossible for the wave run-up on a monopile to be higher than on a wall, the 2D numerical model (waves against a wall) could be used as an upper bound limit for wave run-up heights on monopiles. Together with the relatively fast computation time, it might be usefull in early design of a monopiles. For example when determining the height of the main access platform.

6.3. Explanation of the models

6.3.1. Oceanwave3D

Oceanwave3D has a GUI (Graphical User Interface) where the user can build the model. This to consider are time of the simulation, the time step, the geometry of the domain, the resolution of this domain, stream function input parameters, wave generation and absorption zones. With this input, a input file is created for the simulation in OpenFOAM. This file together with coupling as described in Paulsen et al., 2014 [23] gives the wavefield input of the OpenFOAM simulation.

Due to this coupling it is possible to have the waves running for some time before starting the simulation in OpenFOAM. This means it is possible to get rid of the starting effects of the waves, the waves not being fully developed for example.

6.3.2. OpenFOAM

Within the Oceanwave3D domain, the OpenFOAM domain is created. This is where the actual simulation will take place. For this research a wave flume is created. This wave flume consists of a grid. This grid consists of a number of cells in the x direction and a number of cells in the y direction. Since the problem in this research is 2-dimensional, the number of cells in the z direction is set to 1 cell.

In figure 6.2 a wave flume can be seen, the water is visualized in red and air in blue. OpenFOAM water and air are treated as two different phases with separate densities. The visualization is a representation of the solved cells by the VOF method and either have value of 1 for water, 0 for air. As discussed in chapter 7.1.2.

An example of these cells can be seen in figure 6.3, and the 2D application in figure 6.4.

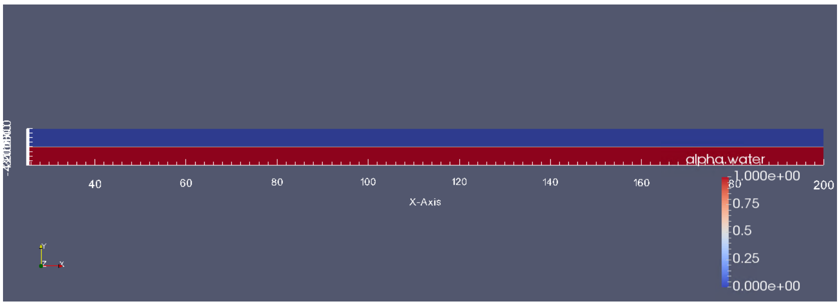

Figure 6.2: Wave flume in OpenFOAM, horizontal and vertical axis are in meters

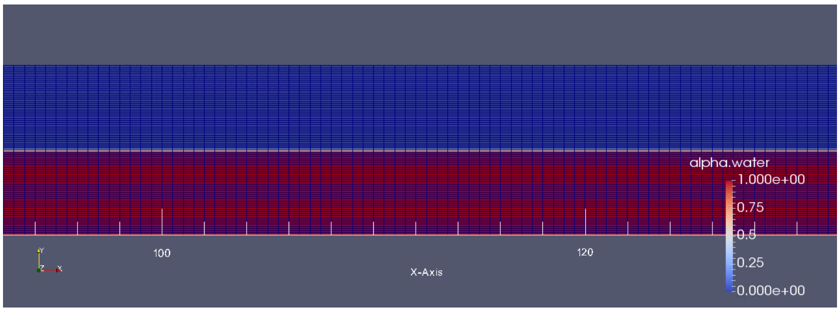

Figure 6.3: Wave flume grid example

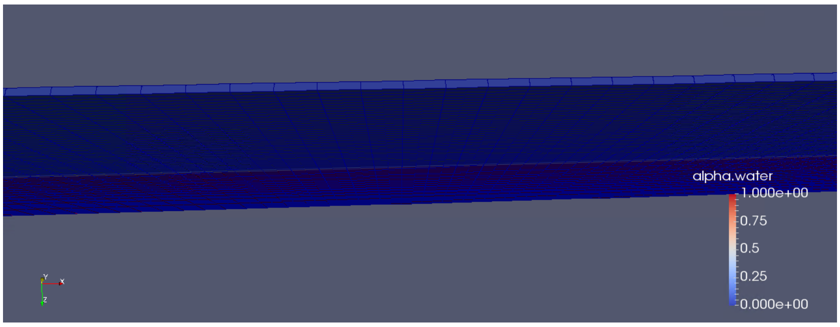

Figure 6.4: Out of plane view of the wave flume, 1 cell in this direction

6.4. Validation of the 2D numerical model

6.4.1. Wave validation

The first step of running the model is to check the wave in the numerical model with the theoretical stream function wave.

In OceanWave3D a regular wave field will be created using non-linear stream function theory. A maximum wave height $H = H_{max}[m]$, maximum wave period $T = T_{hmax}[s]$ and water depth $h[m]$ are inputted. The length of the wave generation zone is chosen to be approximately 1.5 times the corresponding wave length $1.5L$.

In OpenFOAM it is possible to place wave gauges that track the surface elevation of the water. These wave gauges are used to plot the surface elevation of the model against the theoretical stream function waves. At first a smaller wave flume has been investigated to see if the coupling between OceanWave3D and the OpenFOAM domain was done correctly. This smaller flume has a lower computation time and therefore is used in the beginning. The following wave input parameters are used: $H = 0.972m$, $h = 4m$ and $T = 3.76s$. In figure 6.5 a visualization of the waves in the OpenFOAM domain can be seen.

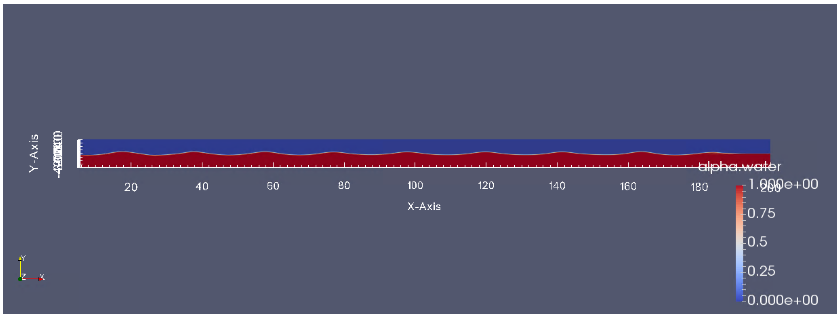

Figure 6.5: Visualization of the wave in the OpenFOAM domain

After this, the surface elevation of the wave gauge is plotted against the theoretical surface elevation of a stream function wave. In figure 6.6 the need for a later start can be seen, the waves need to develop first. The waves, especially from $t = 40s$ show good agreement with the theoretical stream function wave. The order N of the stream function used is 32.

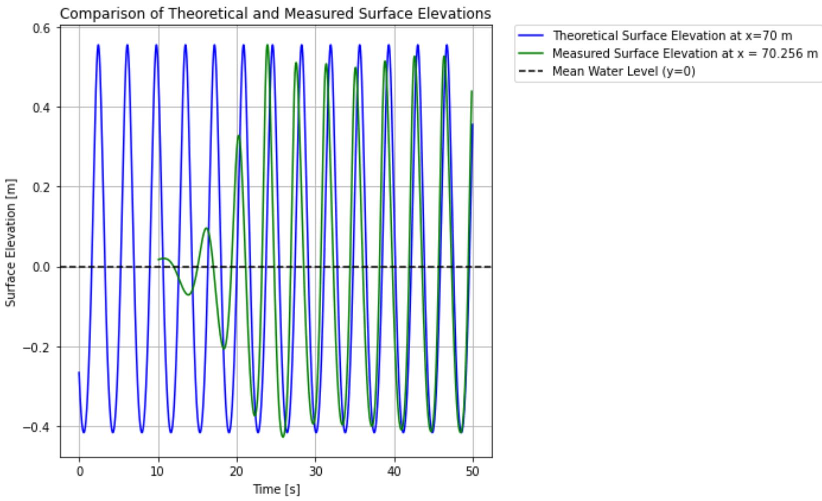

Figure 6.6: Comparison of theoretical and measured surface elevations

The next step is to go to a larger wave flume, the wave input parameters are the following: $H = 13m$, $h = 25m$ and $T = 13s$.

In figure 6.7 a snapshot of the waves in the OpenFOAM simulation can be seen. In the beginning of the wave flume the wave is still in the coupling part, while later in the wave flume the wave is in a normal shape. At the end of the wave flume the wave absorber is also visible.

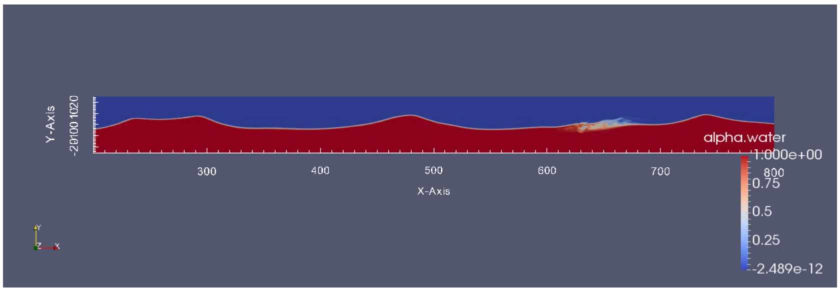

Figure 6.7: Visualization of the large wave flume with H=13m waves.

In figure 6.8 a comparison of the surface elevation at the location the the wave gauge, $x = 480m$ is shown. At first, the wave is off, probably due to starting effects. But after $t = 100s$ the waves are resembling the theoretical wave of the stream function. This figure can be used to choose the starting and end time of the simulation later when the wall is present in the wave flume. Only one wave from trough to trough is needed for such a simulation to measure the wave run-up height on a wall. After this, reflections from the wall will become significant, and a realistic wave run-up height cannot be measured.

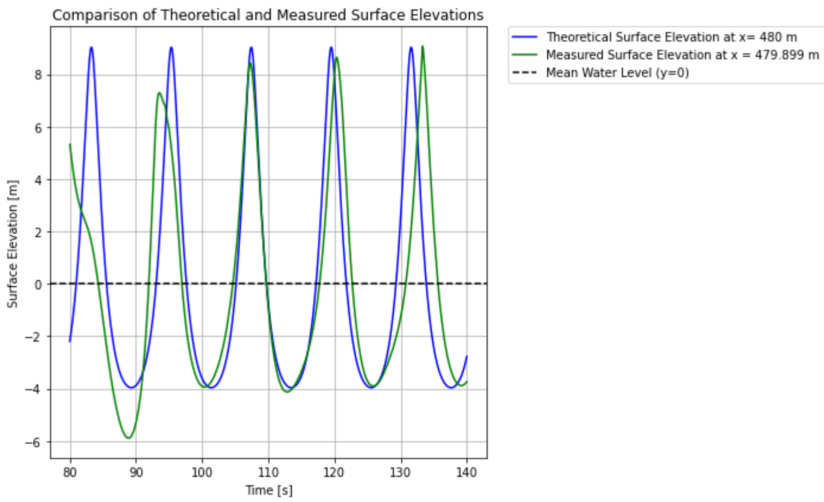

Figure 6.8: Theoretical surface elevation vs simulation H=13m.

6.4.2. Wave run-up height results

First it is investigated if the numerical model performs within range of the theoretical wave run-up limit of a wave against a wall. After this the results of the 2D numerical model will be discussed. The analytical wave run-up models are derived from 3D experiments and can therefore not be compared directly with the wave run-up results from the 2D numerical model. The numerical, however, can provide an upper limit and provide insight into whether the analytical models can be used and whether they are used outside their limits. The results of this numerical model and analytical models are compared to theoretical waves on a wall.

The next step to perform the wave run-up against the wall is to add the wall in the numerical wave flume. The wave run-up heights will be measured with wave gauges in the area before the wall. In figure 6.9 the wave flume with the wall is shown. In figure 6.10 and 6.11 the approach of the wave and the actual wave run-up against the wall can be seen. It can also be observed that in these figure waves are present behind the wall. The reason for this is that the wave are already running through the OpenFOAM domain before the simulation starts. This is because it is desired to let the simulations start at a point in time where the waves are fully developed. Another reason is that the simulation can start when the crest of the wave just passed. Therefore the wall is introduced in a later stage and are waves visible after the wall. The wave input parameters are: $H = 14m$, $h = 25m$ and $T = 13s$.

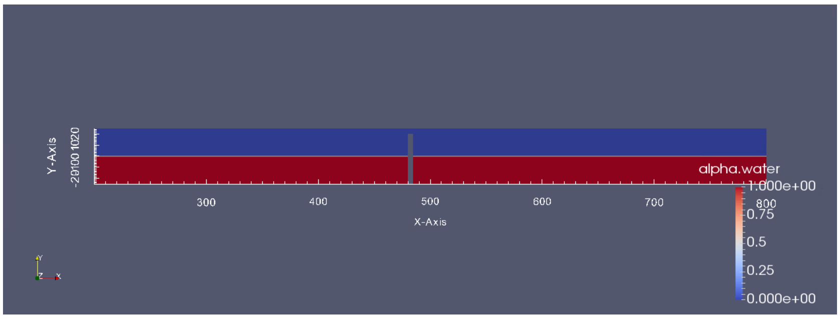

Figure 6.9: Large wave flume with wall

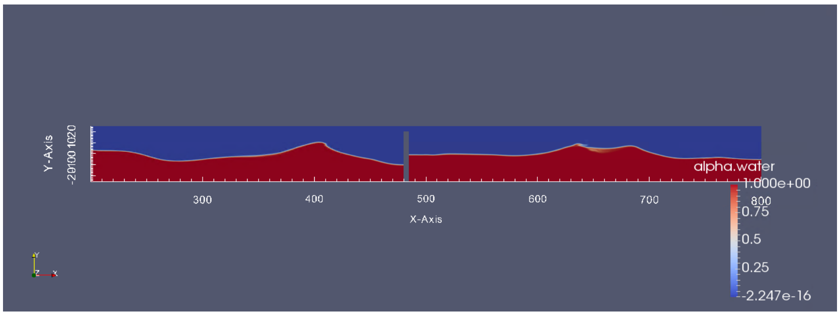

Figure 6.10: Large wave flume with wall - approach of the wave to the wall. The wall is introduced at t=120s

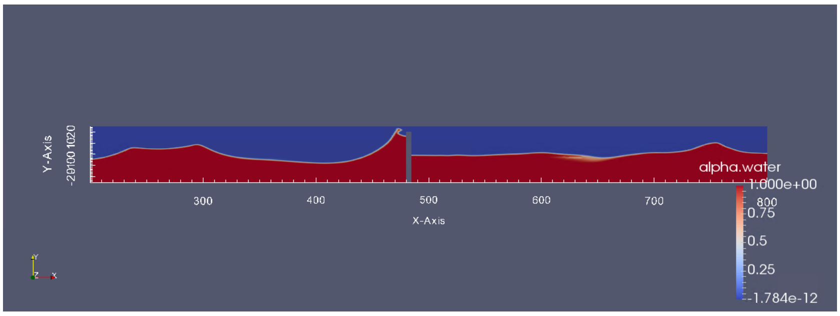

Figure 6.11: Large wave flume with wall - wave run-up on the wall

The wave run-up height on the wall is measured for the following case: $H = 10m, 11m, 12m, 13m, 14m, 15m, 16m$, $h = 25m$ and $T = 13s$. And then compared to the analytical methods and theoretical run-up height limits on a wall.

The surface elevation before the wall is plotted at different locations before the wall, figure 6.12. These wave gauges just before the wall measure the wave run-up height.

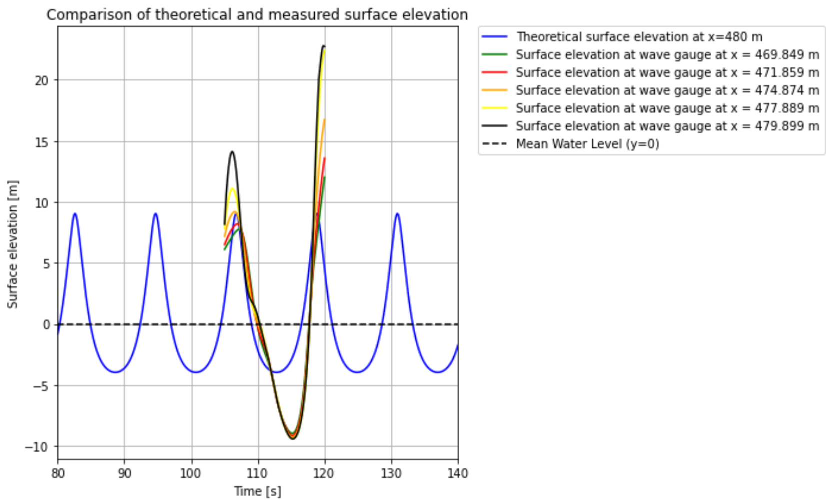

Figure 6.12: The wave run-up height before the wall of H=13m, h=25m and T=13s

From the surface elevation file the wave run-up height of the numerical model is determined. For each wave height, the results are documented in table 6.2 and figure 6.16. In this table the numerical results are compared with the two theoretical wall limits and the analytical wave height models.

For the wave heights $H = 15m$ and $H = 16m$ the wave run-up on the wall is not included in the results since the wave start breaking after leaving the coupling zone. Breaking waves are not included in this research. The surface elevation is plotted below as well as snapshot of the simulation. It can be seen that surface elevation is not in good agreement with the theoretical surface elevation anymore. This has to do with the fact that these waves are too steep for the flat slope of this wave flume and therefore start breaking.

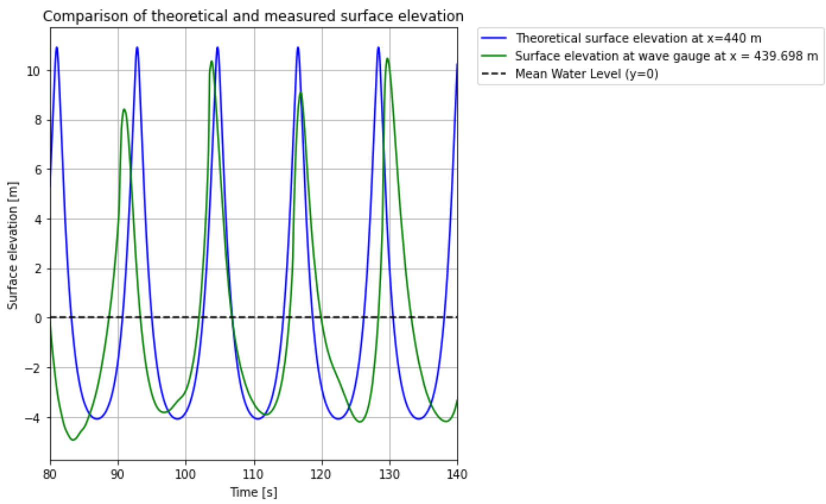

Figure 6.13: Surface elevation at wave gauge at x=440m vs theoretical surface elevation - H=15m, h=25m and T=13s.

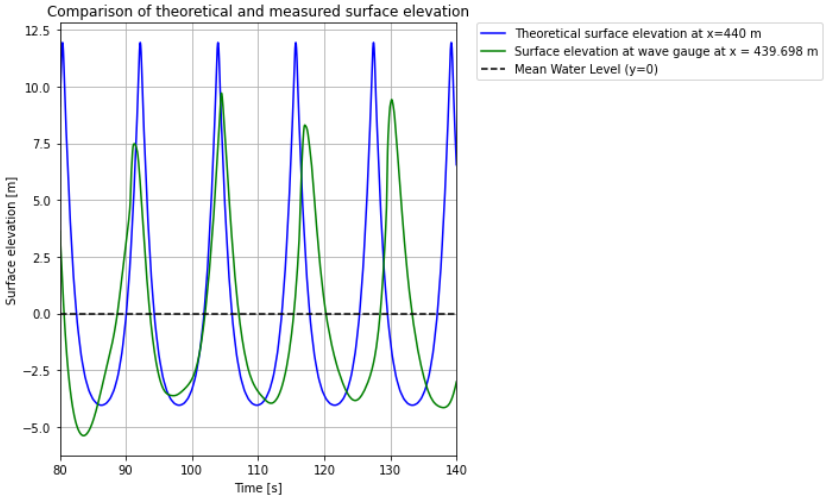

Figure 6.14: Surface elevation at wave gauge at x=440m vs theoretical surface elevation - H=16m, h=25m and T=13s.

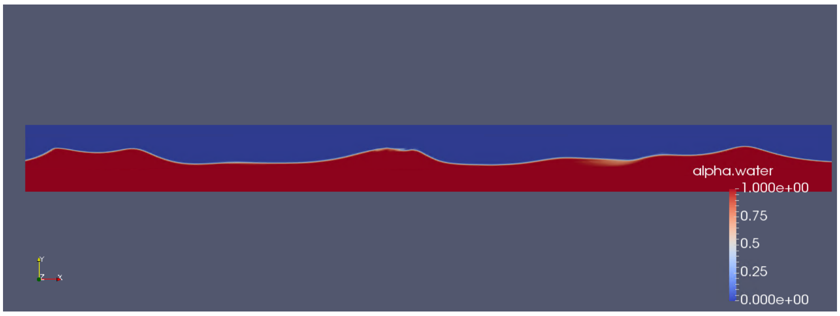

Figure 6.15: Wave breaking in the wave flume for H=16m, h=25m and T=13s.

Table 6.2: Numerical results compared with the theoretical limit of wall and analytical wave run-up models for different wave heights.

(a) Numerical wave run-up, H=10m

Method		**Wave run-up height [m]**
Wave height	H=10m	
Numerical model		17.7
Limit: 2.6*ai		16.9
Limit: EurOtop		12.0
Garborg lvl A		8.5
Garborg lvl B		10.6
Garborg with m=3.5		11.3
de Latour		16.6
Li		7.9

(b) Numerical wave run-up, H=11m

Method		**Wave run-up height [m]**
Wave height	H=11m	
Numerical model		20.2
Limit: 2.6*ai		18.9
Limit: EurOtop		13.2
Garborg lvl A		10.0
Garborg lvl B		12.7
Garborg with m=3.5		13.5
de Latour		18.7
Li		9.1

(c) Numerical wave run-up, H=12m

Method		**Wave run-up height [m]**
Wave height	H=12m	
Numerical model		21.6
Limit: 2.6*ai		21.3
Limit: EurOtop		14.4
Garborg lvl A		11.6
Garborg lvl B		15.0
Garborg with m=3.5		16.3
de Latour		20.7
Li		13.3

(d) Numerical wave run-up, H=13m

Method		**Wave run-up height [m]**
Wave height	H=13m	
Numerical model		23.0
Limit: 2.6*ai		23.3
Limit: EurOtop		15.6
Garborg lvl A		13.5
Garborg lvl B		18.0
Garborg with m=3.5		19.5
de Latour		22.7
Li		11.7

(e) Numerical wave run-up, H=14m

Method		**Wave run-up height [m]**
Wave height	H=14m	
Numerical model		20.4
Limit: 2.6*ai		25.7
Limit: EurOtop		16.8
Garborg lvl A		15.8
Garborg lvl B		21.6
Garborg with m=3.5		23.6
de Latour		24.7
Li		13.3

(f) Numerical wave run-up, H=15m

Method		**Wave run-up height [m]**
Wave height	H=15m	
Numerical model		Wave breaking
Limit: 2.6*ai		28.3
Limit: EurOtop		18.0
Garborg lvl A		18.7
Garborg lvl B		26.4
Garborg with m=3.5		29.0
de Latour		26.7
Li		15.2

(g) Numerical wave run-up, H=16m

Method		**Wave run-up height [m]**
Wave height	H=16m	
Numerical model		Wave breaking
Limit: 2.6*ai		30.9
Limit: EurOtop		19.2
Garborg lvl A		23.1
Garborg lvl B		34.3
Garborg with m=3.5		38.1
de Latour		28.8
Li		17.9

Figure 6.16: Overview of wave run-up heights

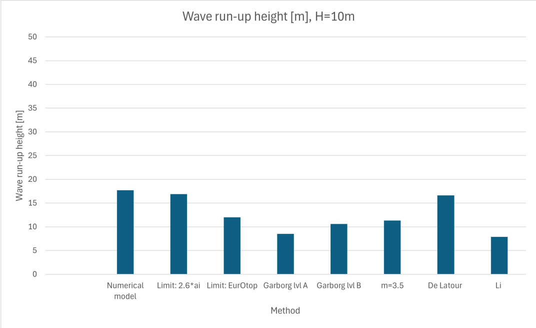

(a) Wave run-up heights for H=10m

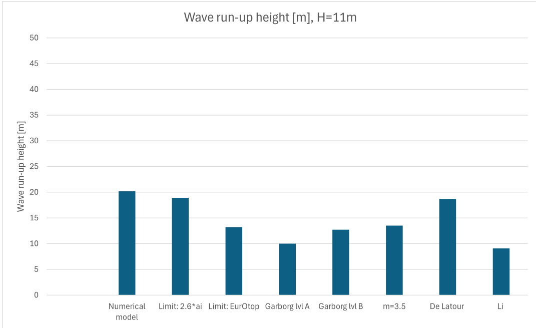

(b) Wave run-up heights for H=11m

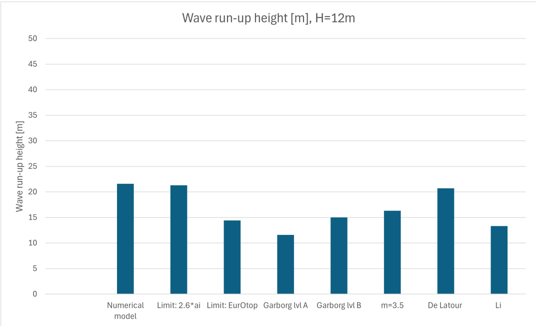

(c) Wave run-up heights for H=12m

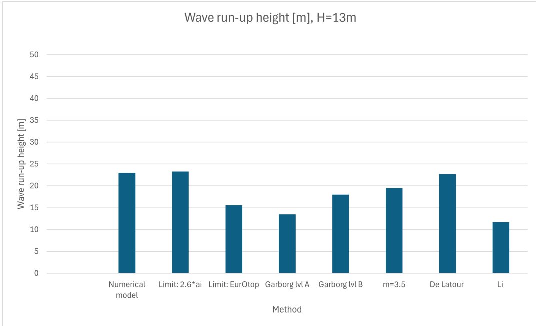

(d) Wave run-up heights for H=13m

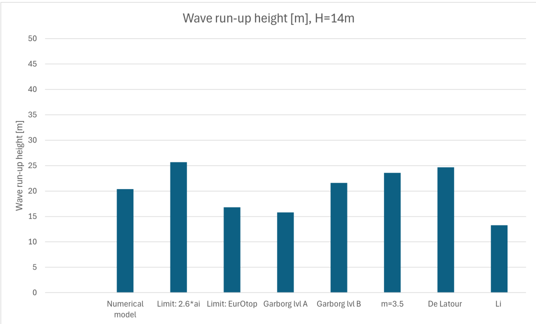

(e) Wave run-up heights for H=14m

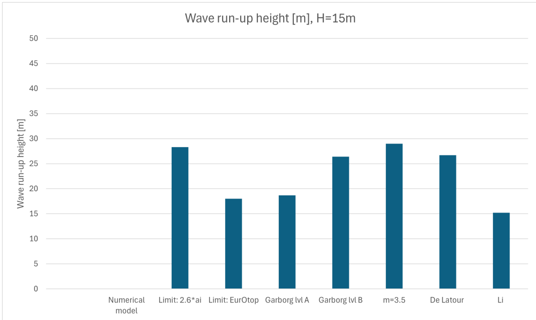

(f) Wave run-up heights for H=15m

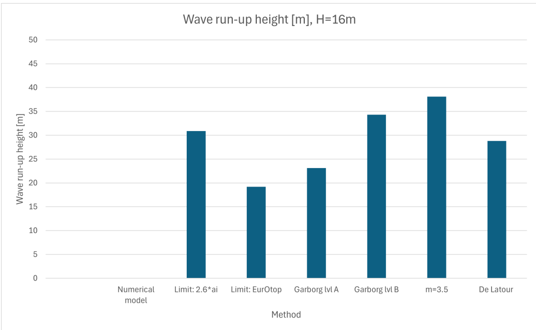

(g) Wave run-up heights for H=16m

6.5. Discussion of the results

In this chapter, the comparison between the numerical results, the limits, and analytical models is discussed.

- First of all, it can be concluded that the theoretical wave run-up height of the EurOtop limit [27] $Ru = 1.8H_{m0}$ is lower than the limit from Ning et al., [22] $Ru = 2.6a_i$. A possible reason for this is that in the study done by Ning, regular waves are used. While the EurOtop manual uses irregular waves. Irregular waves can be considered as resulting in less run-up height because more energy is dissipated due to local steepness for example.
- The results of the numerical simulations are always higher than the theoretical limit of the EurOtop manual.
- The results of the numerical simulations are sometimes higher than the limit of $2.6 * a_i$ and sometimes lower. For all simulations except $H = 14m$ they are within a range of 10% of this limit. For $H = 15m$ and $H = 16m$ the wave run-up height results are not included because of wave breaking.
- The method of de Latour is almost the same as the theoretical limit of a wall for all wave heights. The method can be considered as conservative because it calculates waves run-up on a cylinder instead of a wall.
- The methods of Li and Garborg level A (thick layer run-up), are within the limit of a wall for all cases.
- The method of Garborg level B and the conservative method with $m = 3.5$ start to exceed the theoretical wave limit from a wave height of $H = 15m$. This is because of the dominant particle velocity in these equations and a higher value of m, meaning the wave run-up height increases fast when the wave height increases. The H/h ratio is 0.6 at that moment, so beyond the boundary of the experiments where these equations are validated with. The high H/h ratio for the experiments used for those equations is 0.46.

7 Conclusion

This chapter answers the sub-questions and the main research question of this research.

7.1. Sub-questions

7.1.1. How do the analytical wave run-up height models compare to each other?

In this research the following analytical models are compared with each other, all equations can be found in table 3.1:

- A method developed by de Latour, 2017 [6] with the wave run-up height experiments performed during WIFI JIP II. This method calculates wave run-up heights on a cylinder based on empirical formulas with the maximum wave height, water depth, wave length and diameter of the cylinder.
- A method developed by Garborg et al., 2020 [12] where they re-analyse experiments. This method is based on the velocity stagnation theory and calibrated to the experiments by a run-up coefficient m. This m-value is 1.5 for thin layer run-up on the cylinder and m is 3 for thick layer run-up on the cylinder.
- A method where m=3.5 is used for conservatism, 2022 [9].It uses the same equation as Garborg et al, but they use a value of m is 3.5 for conservatism.
- The last method is from Li et al., 2022 [18] they also use the velocity stagnation theory but re-evaluated the wave run-up coefficient m. In their research m depends on the wave and structural parameters.

All analytical models are used to calculate the wave run-up heights of 100 locations within a wind-farm. At each location the maximum wave run-up height is calculated with the maximum wave height, water depth at the location and the wave period that gives the highest wave run-up ($T = 11.4 - 18s$). The results can be seen in figure 3.5.

From these results the following conclusions can be drawn:

- The resulting wave run-up height of the method of de Latour is less sensitive to changes in wave height than the other methods.
- The particle velocity is very dominant in the outcome of the wave run-up height in the methods of Garborg and the conservative method with $m = 3.5$. The combination of this value being squared in the run-up height equation and the high values of the wave run-up coefficient m gives wave run-up height values as high as $60m$.
- The method of Li gives the lowest results in wave run-up height. This is because the parameter dependent wave run-up coefficient m they introduced is below 1.0 for a wave height of around $8m$ or higher. This reduces the effect the particle velocity has on the wave run-up height.
- The wave run-up heights of Garborg level B and the conservative method with $m = 3.5$ are extremely high and are not considered realistic.

- Another reason for Li's lower results could be the difference in experimental approach. Li uses regular wave experiments to calibrate their results, whereas Garborg and de Latour use irregular wave experiments. This difference could explain the differences between the methods, as regular waves do not capture the nonlinearities present in irregular wave fields and may therefore underestimate wave run-up height.

When taking a closer look to the waves that cause these extreme wave run-up heights, it is concluded that these waves do not satisfy all criteria (a wave that satisfies the boundary conditions, requirements of convergence and consistency). In figure 3.12 and 3.13 the particle velocity and surface elevation of the wave that gives these wave run-up are shown. In these figures it can be seen that the order of the stream function influences the outcome of the particle velocity and surface elevation. Double crests are observed as well as peaks at different locations in time. It can be concluded that this wave is not correct.

Another reason for these extreme wave run-up heights is that the extreme waves that are used for this research are beyond the boundaries where these models are validated. It is important to use additional checks when working with extreme waves. The H/h limits of the analytical models can be found in table 4.1. If the waves exceeds the high boundary of the H/h limit of the experiments the reliability of the results cannot be guaranteed. All Dogger Bank locations are above the line as shown in figure 4.16 and discussed in section 4.3. Therefore, additional limits are needed to make sure more reliable results can be obtained.

The two main limits are suggested to obtain more realistic wave run-up heights are the following:

- The wave height of the extreme waves is lowered until wave length convergence is reached. When doing this more realistic waves are used in the wave run-up height equations.
- A theoretical limit of waves against a wall can be used as an upper bound limit for wave run-up on a cylinder. It is physically not likely for a wave to have higher wave run-up on a cylinder than wave run-up on a wall. This is due to the 3D effect of water dissipating around the cylinder. In this research this limit is taken as 2.6 times the incoming wave amplitude as described in Ning et al., 2017 [22].

All above conclusions considered, it is best to use Garborg level B for wave run-up with H/h ratios up until $H/h = 0.46$ because it is the only method that uses large scale experiments and they were able to create waves with highest H/h values. Above $H/h = 0.46$ it is better to use de Latour, especially for the extreme waves. De Latour does not use stream function theory in the equation and it is a way to avoid high particle velocities (u) in combination with high run-up coefficients (m) which leads to high wave run-up for Garborg. For the extreme waves, de Latour without a limit is approximately the same as the limit for wave run-up on a wall, so conservative. If the goal is to be less conservative, one of the two limits to lower the wave height can be considered to get lower wave run-up results.

7.1.2. How are the wave run-up heights translated into loads?

After calculating wave run-up heights the next step in the analytical approach is to translate these wave run-up heights into wave run-up loads. For analytical model this is done with the following two steps:

1. Calculate the vertical wave run-up velocity at a reference height z, $v(z) = \sqrt{2g \cdot (R_u - z)}$. This reference height z should be chosen at the desired main access platform height.
2. With this vertical wave run-up velocity the pressure on the horizontal platform can be calculated: $\frac{F}{A} = \frac{1}{2} C_s \rho (v(z))^2$. This equation includes a slamming coefficient C_s, these can be derived from a graph developed by Damsgaard et al., 2007 [5]. This graph is derived by measured pressure on a horizontal platform during experiments. Two different pressures are calculated: global pressure and local pressure. The local wave run-up loads are defined as the pressure over an area of $0.5m^2$, the middle of this area is taken $2m$ from the monopile edge. The global wave run-up loads are defined as the pressure over the main access platform over an area of 160°, where the middle is defined as the wave direction. Illustration of both pressure can be found in figures 3.8 and 3.9.

Other analytical methods to translate wave run-up heights into wave run-up loads were not found.

In OpenFOAM it is possible to measure forces on the surface of a structure. It is however not possible to validated these results due to a lack of experiment. Therefore it is not possible to say something about the reliability of these results.

7.1.3. How does a numerical model in OpenFOAM compare to these analytical models?

A 2-dimensional numerical model is created to calculate the wave run-up height on a wall. This model is used as an upper bound limit for the wave run-up height since it is physically unlikely for wave run-up on a cylinder to be higher than wave run-up on a wall. The results from this model are compared to two theoretical limits of wave run-up on a wall and to the analytical models.

- The wave run-up on the wall of the 2-dimensional model is within 10% of the theoretical wall wave run-up of $2.6a_i$ for wave heights up until $H = 13m$.
- The wave run-up on the wall of the 2-dimensional model is higher than the EurOtop limit of $R_u = 1.8H_{m0}$ for all cases. This limit is lower than the other wall limit because the significant wave height is used instead of maximum wave height, all wave heights used in the simulations need to be corrected before the run-up is calculated.
- The method of Garborg level B and the conservative method with $m = 3.5$ start to exceed the theoretical wave limit from a wave height of $H = 15m$. This is because of the dominant particle velocity in these equations and a higher value of m, meaning the wave run-up height increases fast when the wave height increases. The H/h ratio is 0.6 at that moment, so beyond the boundary of the experiments where these equations are derived for, see table 4.1. The highest H/h ratio for the experiments used for those equations is 0.46.
- The method of de Latour is almost the same as the theoretical limit of a wall for all wave heights. The method can be considered as conservative because it calculates waves run-up on a cylinder instead of a wall.
- The methods of Li and Garborg level A (thick layer run-up), are within the limit of wall for all analysed cases.

7.1.4. Is it possible to make a simple model to obtain reasonable accurate predictions of wave run-up loads within a time span of a few days?

In this research two different kind of models are developed to see if it is possible to make a time-efficient model that can predict reasonable accurate predictions for wave run-up loads. The first one is an analytical model where different approaches are compared and limits on these approaches are investigated.

First of all, better insight in the different analytical models is provided in this research. With the obtained limits in this research, a better insight is given in when the analytical are used outside its boundaries and provides methods to reduce the risk of unreliable results. Since there is only one analytical method found to translate wave run-up heights into wave run-up loads, the same can be said about the loads. However it is advised to gain more insight into this translation of wave run-up height into wave run-up loads. It could be that this translation is very conservative, but since there was no way to compare methods this is for further research.

Secondly, a 2-dimensional model is created to calculate the wave run-up height on a wall. This model can be used as an upper bound limit of the wave run-up height on a cylinder since it is physically unlikely for wave run-up on a cylinder to be higher than on a wall.

No 2-dimensional numerical was found in this thesis to calculate validated loads on a platform.

7.2. Main research question

7.2.1. How can CFD modeling in OpenFOAM be applied to determine the wave run-up loads on the main access platform of a monopile in early design stage and how do CFD models compare to existing analytical models?

The goal of this research is to investigate if a relatively quick numerical model can contribute to more accurate wave run-up results and how such a model compares to existing analytical wave run-up models.

A 2-dimensional numerical model (waves on wall) can be used to help determine the reliability of the waves that are outside the boundaries of the analytical models. Since the $2.6a_i$ limit is in the same range as the numerical, it is more time efficient to use this wall limit. When waves are used outside the boundaries of the analytical models the waves run-up height and therefore load results increase a lot faster than the numerical and theoretical results on a wall. It can be used as a check not to exceed limit for the analytical wave run-up models.

Within the use of the analytical wave run-up models themselves new insights has been discovered as well. The most important one is that the reliability of the waves run-up results goes down when the H/h ratio for the experiments has been exceeded. Limits have been investigated to increase the reliability again.

8 Recommendations

This research provides further understanding on how to predict wave run-up heights and loads on a main access platform in a relatively small amount of time. There is however still a lot that can be improved, some recommendations are given in this chapter.

8.1. Analytical model

- At this moment there is only one method to translate wave run-up heights into wave run-up loads, this method has been validated with one set of experiments. There are no other experiments performed on wave run-up loads on a horizontal platform. It is necessary to further investigate the slamming coefficient that needs to be used in the final equation that calculates the loads.
- To further improve the reliability of the analytical models for extreme waves it is necessary to perform experiments with H/h ratios higher than that are available now. The existing wave run-up height models can be further calibrated to these extreme conditions.

8.2. Numerical model

- The 2-dimensional model used in this thesis could be extended with a platform at the top and measure loads. However, there is no way to validate these results. In order to use such a model validation of these loads is needed with experiments.
- With a validated 2D model and a validated 3D model, an investigation into the differences between 2D and 3D numerical modeling could be done. A link between 2D and 3D could be made.
- In this 2-dimensional model there is no way to validate wave run-up loads on a platform. This means the reliability of 2-dimensional cannot be compared to any other results and therefore cannot be used as limit for the loads. Also measuring pressures on a platform on a wall could be helpful to further understand this.

Bibliography

[1] Dogger Bank. Input to Site Conditions Assessment Marine Assessment. Technical report.

[2] N. Abdussamie, W. Amin, R. Ojeda, and G. Thomas. Vertical Wave-in-Deck Loading and Pressure Distribution on Fixed Horizontal Decks of Offshore Platforms. 2014.

[3] L. Bonakdar, H. Oumeraci, and A. Etemad-Shahidi. Run-up on vertical piles due to regular waves: Small-scale model tests and prediction formulae. *Coastal Engineering*, 118:1–11, 12 2016. ISSN 03783839. doi: 10.1016/j.coastaleng.2016.08.008.

[4] H. Bredmose and N. G. Jacobsen. Vertical Wave Impacts on Offshore Wind Turbine Inspection Platforms. Technical report, 2011.

[5] M. L. Damsgaard, H. Gravesen, and T. L. Andersen. Design loads on platforms on offshore wind turbine foundations with respect to vertical wave run-up. Technical report, 2007. URL `https://www.researchgate.net/publication/249993799`.

[6] T. de Latour. WIFI JIP-INTERNSHIP REPORT Run-up on wind turbines II. Technical report, Marin, 2017.

[7] L. De Vos, P. Frigaard, and J. De Rouck. Wave run-up on cylindrical and cone shaped foundations for offshore wind turbines. Technical report, 2007.

[8] DNV. DNV-RP-C205 Environmental conditions and environmental loads. Technical report, 2019.

[9] Dogger Bank Wind Farm. Wave Run-up study. Technical report.

[10] A. P. Engsig-Karup, H. B. Bingham, and O. Lindberg. An efficient flexible-order model for 3D nonlinear water waves. *Journal of Computational Physics*, 228(6):2100–2118, 4 2009. ISSN 10902716. doi: 10.1016/j.jcp.2008.11.028.

[11] J. D. Fenton. THE NUMERICAL SOLUTION OF STEADY WATER WAVE PROBLEMS. Technical Report 3, 1988.

[12] K. Garborg, T. Lykke Andersen, J. Skourup, and P. B. Frigaard. Re-Analysis of Run-Up Levels for Slender Monopiles. *International Journal of Ocean and Coastal Engineering*, 02(01n02), 3 2019. ISSN 2529-8070. doi: 10.1142/s2529807019500027.

[13] J. Grue and B. Osyka. Runup on a vertical column in strong water wave events. *Coastal Engineering*, 163, 1 2021. ISSN 03783839. doi: 10.1016/j.coastaleng.2020.103775.

[14] R. J. Hallermeier. Nonlinear Flow of Wave Crests Past a Thin Pile. *Journal of the Waterways Harbors and Coastal Engineering Division*, 1976.

[15] L. H. Holthuijsen. Waves in Oceanic and Coastal Waters. Technical report, 2007.

[16] N. G. Jacobsen, D. R. Fuhrman, and J. Fredsøe. A wave generation toolbox for the open-source CFD library: OpenFoam®. *International Journal for Numerical Methods in Fluids*, 70(9):1073–1088, 11 2012. ISSN 02712091. doi: 10.1002/fld.2726.

[17] M. H. Kazeminezhad and A. Etemad-Shahidi. A new method for the prediction of wave runup on vertical piles. *Coastal Engineering*, 98:55–64, 4 2015. ISSN 03783839. doi: 10.1016/j.coastaleng.2015.01.004.

[18] J. Li, X. Ji, L. Yue, and S. Liu. An improved method for calculating the wave run-up on a vertical cylinder based on the velocity stagnation head theory. *Ocean Engineering*, 266, 12 2022. ISSN 00298018. doi: 10.1016/j.oceaneng.2022.112915.

[19] T. Lykke Andersen and M. Brorsen. Horns Rev II, 2D-Model Tests Impact Pressures on Horizontal and Cone Platforms from Irregular Waves. Technical report, 2007.

[20] T. Lykke Andersen, P. Frigaard, M. L. Damsgaard, and L. De Vos. Wave run-up on slender piles in design conditions - Model tests and design rules for offshore wind. *Coastal Engineering*, 58(4): 281–289, 4 2011. ISSN 03783839. doi: 10.1016/j.coastaleng.2010.10.002.

[21] J. M. Niedzwecki and A. S. Duggal. WAVE RUNUP AND FORCES ON CYLINDERS IN REGULAR AND RANDOM WAVES. Technical report, 1992.

[22] D. Ning, R. Wang, L. Chen, J. Li, J. Zang, L. Cheng, and S. Liu. Extreme wave run-up and pressure on a vertical seawall. *Applied Ocean Research*, 67:188–200, 9 2017. ISSN 01411187. doi: 10.1016/j.apor.2017.07.015.

[23] B. T. Paulsen, H. Bredmose, and H. B. Bingham. An efficient domain decomposition strategy for wave loads on surface piercing circular cylinders. *Coastal Engineering*, 86:57–76, 4 2014. ISSN 03783839. doi: 10.1016/j.coastaleng.2014.01.006.

[24] D. Pavilons, V. Hengelmolen, D. Plenker, N. Bruinsma, L. Biermans, A. Smale, and P. Wellens. Hydrodynamic loading of breaking waves of breaking waves on offshore inspection platforms Thesis Hydrodynamic loading of breaking waves on offshore in-spection platforms. Technical report, 2022.

[25] Z. Peng, P. Wellens, and T. Raaijmakers. 3-D numerical modeling of wave run-up on monopiles. In *Proceedings of the International Conference on Offshore Mechanics and Arctic Engineering - OMAE*, volume 5, pages 327–335, 2012. ISBN 9780791844922. doi: 10.1115/OMAE2012-83858.

[26] J. Ramirez, P. Frigaard, T. Lykke Andersen, and L. de Vos. Large scale model test investigation on wave run-up in irregular waves at slender piles. *Coastal Engineering*, 72:69–79, 2 2013. ISSN 03783839. doi: 10.1016/j.coastaleng.2012.09.004.

[27] J. Van der Meer, N. Allsop, T. Bruce, J. De Rouck, A. Kortenhaus, T. Pullen, H. Schüttrumpf, P. Troch, and B. Zanuttigh. EurOtop Manual on wave overtopping of sea defences and related structures An overtopping manual largely based on European research, but for worldwide application Second Edition 2018. Technical report, 2018. URL `www.overtopping-manual.com`.

A

Numerical wave run-up

In this appendix more figure and graphs of the numerical wave run-up are presented.

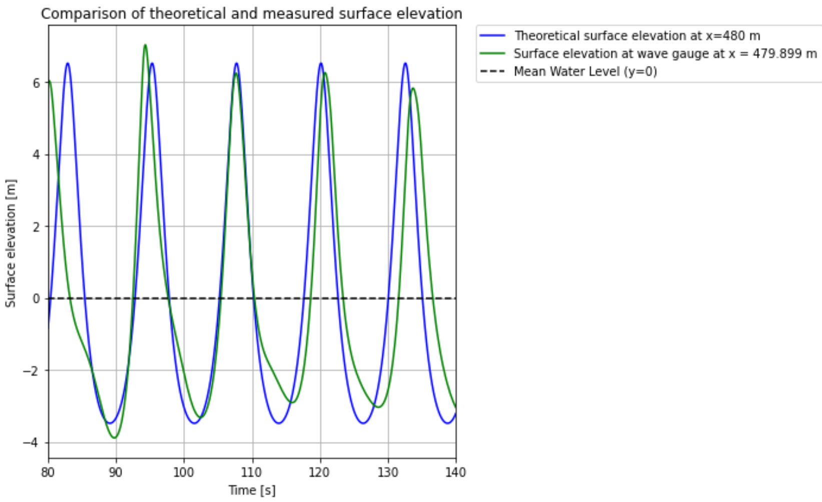

Figure A.1: Surface elevation at wave gauge at x=480m vs theoretical surface elevation - H=10m, h=25m and T=13s.

.

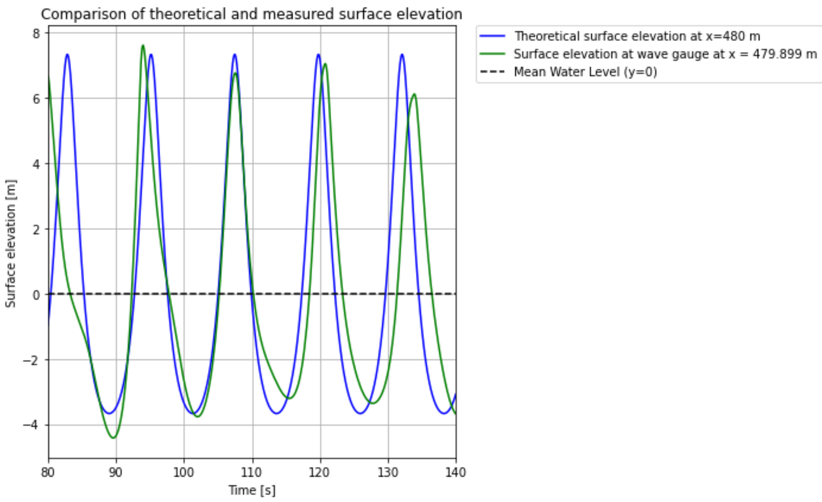

Figure A.2: Surface elevation at wave gauge at x=480m vs theoretical surface elevation - H=11m, h=25m and T=13s.

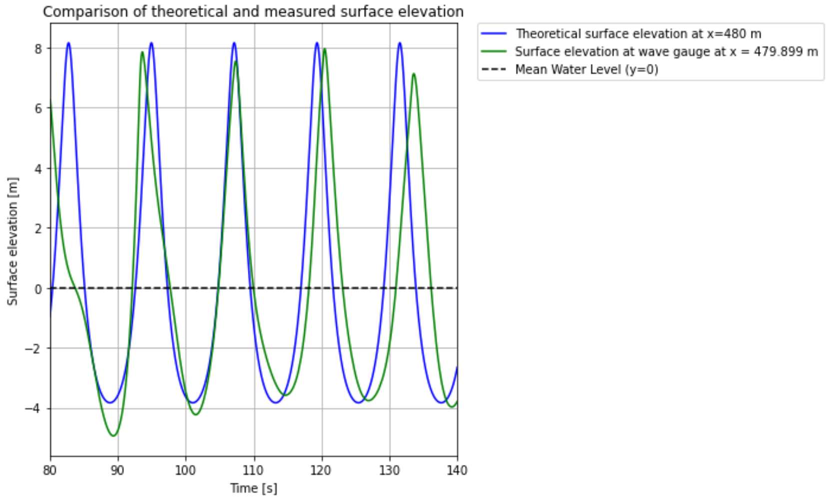

Figure A.3: Surface elevation at wave gauge at x=480m vs theoretical surface elevation - H=12m, h=25m and T=13s.

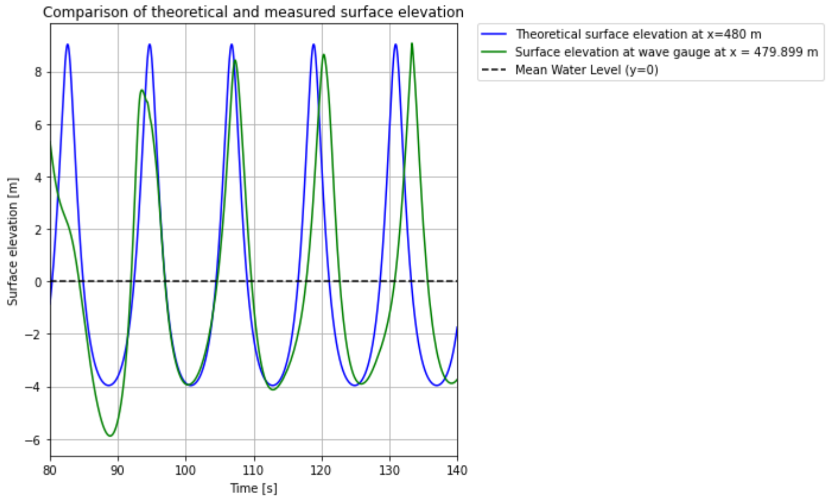

Figure A.4: Surface elevation at wave gauge at x=480m vs theoretical surface elevation - H=13m, h=25m and T=13s.

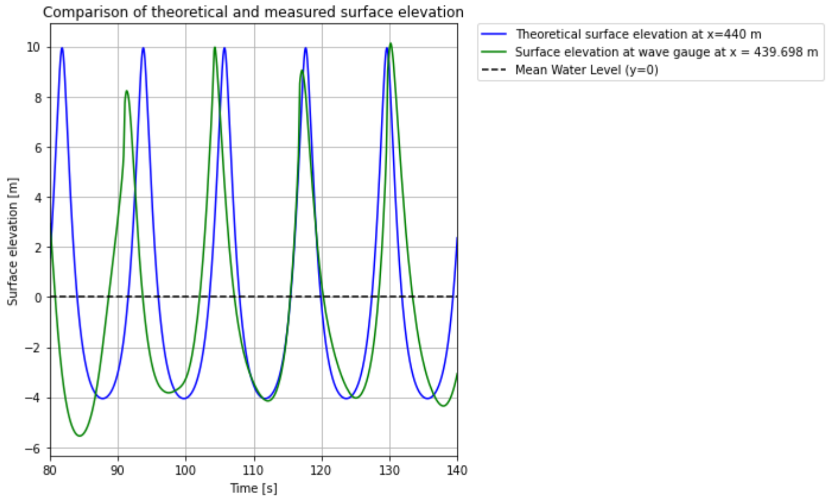

Figure A.5: Surface elevation at wave gauge at x=440m vs theoretical surface elevation - H=14m, h=25m and T=13s.

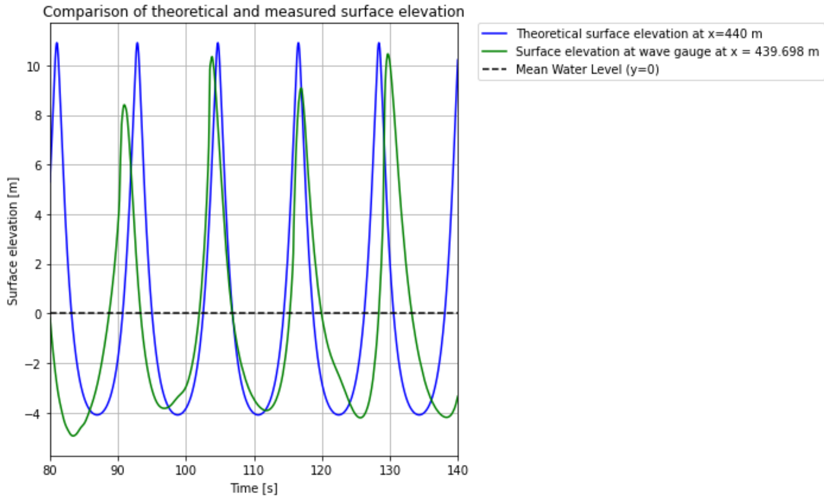

Figure A.6: Surface elevation at wave gauge at x=440m vs theoretical surface elevation - H=15m, h=25m and T=13s.

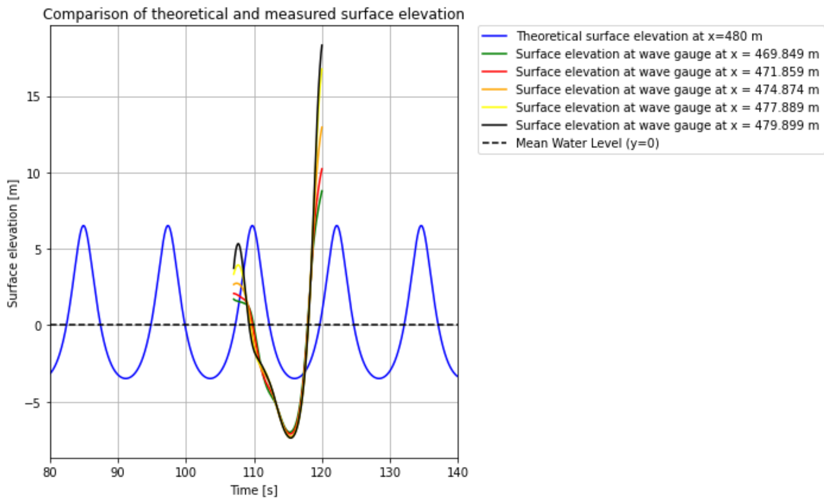

Figure A.7: Surface elevation at the wall for different wave gauge locations locations - H=10m, h=25m and T=13s.

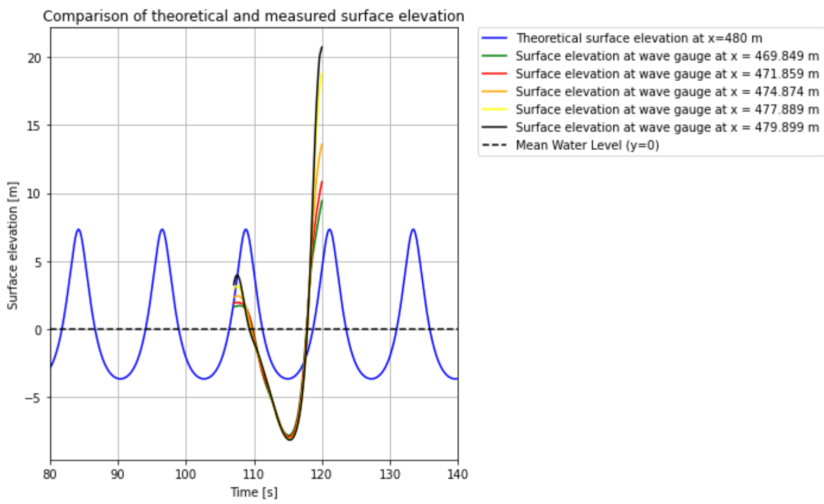

Figure A.8: Surface elevation at the wall for different wave gauge locations locations - H=11m, h=25m and T=13s.

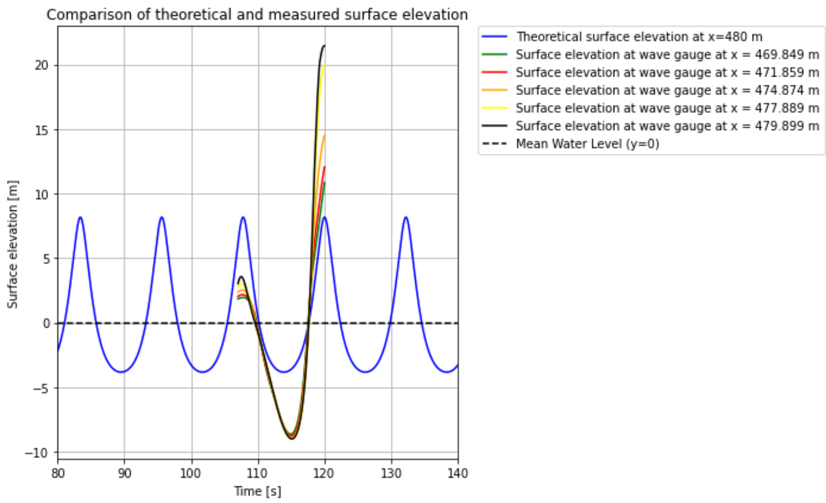

Figure A.9: Surface elevation at the wall for different wave gauge locations locations - H=12m, h=25m and T=13s.

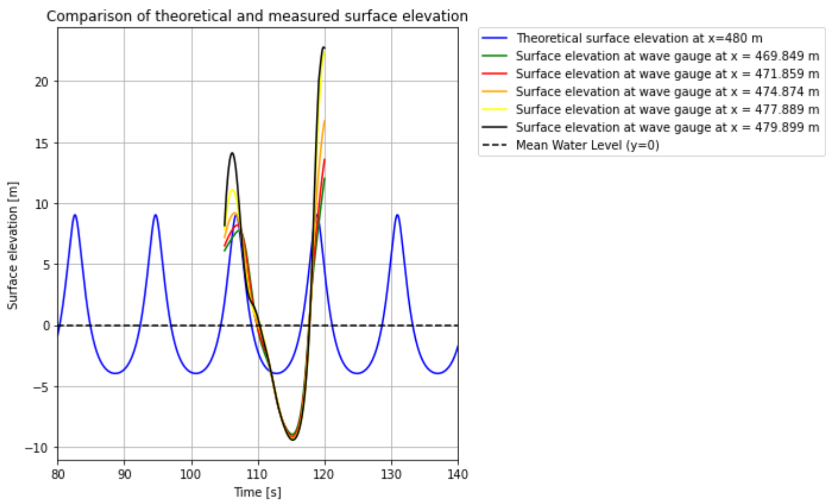

Figure A.10: Surface elevation at the wall for different wave gauge locations locations - H=13m, h=25m and T=13s.